Double Belt Structure of Discoidal High Density Lipoproteins: Molecular Basis for Size Heterogeneity

ARTICLE *in* JOURNAL OF MOLECULAR BIOLOGY · DECEMBER 2004

Impact Factor: 4.33 · DOI: 10.1016/j.jmb.2004.09.017 · Source: PubMed

9 AUTHORS, INCLUDING:

Dongfeng Cao
University of Minnesota Twin Cities
21 PUBLICATIONS **2,021** CITATIONS
SEE PROFILE

Stephen C Harvey
Georgia Institute of Technology
200 PUBLICATIONS **7,319** CITATIONS
SEE PROFILE

Gm Anantharamaiah
University of Alabama at Birmingham
204 PUBLICATIONS **11,428** CITATIONS
SEE PROFILE

Jere Segrest
University of Alabama at Birmingham
204 PUBLICATIONS **11,676** CITATIONS
SEE PROFILE

doi:10.1016/j.jmb.2004.09.017 J. Mol. Biol. (2004) 343, 1293–1311

JMB

Available online at www.sciencedirect.com

SCIENCE DIRECT®

ELSEVIER

Double Belt Structure of Discoidal High Density Lipoproteins: Molecular Basis for Size Heterogeneity

Ling Li[1,2]*, Jianguo Chen[1,2], Vinod K. Mishra[1,2], Jennifer A. Kurtz[1,2] Dongfeng Cao[1,2], Anthony E. Klon[3], Stephen C. Harvey[3] G. M. Anantharamaiah[1,2,3] and Jere P. Segrest[1,2,3]*

[1]*Department of Medicine UAB Medical Center Birmingham, AL 35294, USA*

[2]*Atherosclerosis Research Unit UAB Medical Center Birmingham, AL 35294, USA*

[3]*Department of Biochemistry and Molecular Genetics, UAB Medical Center, Birmingham AL 35294, USA*

**Corresponding authors*

We recently proposed an all-atom model for apolipoprotein (apo) A-I in discoidal high-density lipoprotein in which two monomers form stacked antiparallel helical rings rotationally aligned by interhelical salt-bridges. The model can be derived *a priori* from the geometry of a planar bilayer disc that constrains the hydrophobic face of a continuous amphipathic α helix in lipid-associated apoA-I to a plane inside of an α-helical torus. This constrains each apoA-I monomer to a novel conformation, that of a slightly unwound, curved, planar amphipathic α11/3 helix (three turns per 11 residues). Using non-denaturing gradient gel electrophoresis, we show that dimyristoylphosphocholine discs containing two apoA-I form five distinct particles with maximal Stokes diameters of 98 Å (R2-1), 106 Å (R2-2), 110 Å (R2-3), 114 Å (R2-4) and 120 Å (R2-5). Further, we show that the Stokes diameters of R2-1 and R2-2 are independent of the N-terminal 43 residues (the flexible domain) of apoA-I, while the flexible domain is necessary and sufficient for the formation of the three larger complexes. On the basis of these results, the conformation of apoA-I on the R2-2 disc can be modeled accurately as an amphipathic helical double belt extending the full length of the lipid-associating domain with N and C-terminal ends in direct contact. The smallest of the discs, R2-1, models as the R2-2 conformation with an antiparallel 15–18 residue pairwise segment of helixes hinged off the disc edge. The conformations of full-length apoA-I on the flexible domain-dependent discs (R2-3, R2-4 and R2-5) model as the R2-2 conformation extended on the disc edge by one, two or three of the 11-residue tandem amphipathic helical repeats (termed G1, G2 and G3), respectively, contained within the flexible domain. Although we consider these results to favor the double belt model, the topographically very similar hairpin-belt model cannot be ruled out entirely.

Keywords: apolipoprotein A-I; discoidal high-density lipoprotein; size heterogeneity; double belt model; hairpin-belt model

Introduction

It is now well established that the major apolipoprotein A-I (apo A-I) containing lipoprotein, high-density lipoprotein (HDL), is a negative risk factor for cardiovascular disease.[1,2] ApoA-I is an integral component of both spheroidal circulating HDL particles and the geometrically simpler discoidal nascent HDL particles and largely determines their structure and function. The antiatherogenic properties of HDL relate, in part, to HDL's role in reverse cholesterol transport, the removal of cholesterol

Abbreviations used: apo, apolipoprotein; HDL, high-density lipoprotein; ABCA1, ATP-binding cassette transporter A1; LCAT, lecithin cholesterol acyltransferase; SR-B1, scavenger receptor class B, type I; DMPC, dimyristoylphosphatidylcholine; MD, molecular dynamics; NDGGE, non-denaturing gradient gel electrophoresis; POPC, 1-palmitoyl-2-oleoyl-phosphatidylcholine; MLV, multilamellar vesicles.

E-mail addresses of the corresponding authors: lili@uab.edu; segrest@uab.edu

0022-2836/$ - see front matter

from peripheral tissues for transport to the liver for excretion.

Nascent HDL particles are found in increased concentrations in interstitial tissues as products of an early stage of reverse cholesterol transport.[3] These particles are the products of the interaction of lipid-poor apoA-I with the transmembrane protein, ATP-binding cassette transporter A1 (ABCA1),[4–8] on the surface of fibroblasts and other cellular components of interstitial tissues.[9] During further steps in reverse cholesterol transport, once the discoidal particles reach plasma, apoA-I activates lecithin cholesterol acyltransferase (LCAT), resulting in cholesterol esterification and conversion to spheroidal HDL for transport to the liver and interaction with scavenger receptor class B, type I (SR-B1), and other receptors for cholesterol excretion.

ApoA-I functions depend upon its unique structural properties (Figure 1). Mature human apoA-I is a 243 residue protein that contains a lipid-associating C-terminal domain (residues 44–243);[10] the amino acid residues 1–43 (termed the flexible domain) are encoded by exon 3, whereas the lipid-associating domain is encoded by exon 4 of the apoA-I gene. It is known that there are eight 22mer and two 11mer tandem amino acid sequence repeats, often punctuated by praline residues, in the lipid-associating domain (designated helixes 1–10); each repeat has the periodicity of a class A amphipathic α helix.[10,11] The N-terminal flexible domain contains three 11mer tandem repeats (residues 11–21, 22–32 and 33–43, termed helixes G1, G2 and G3, respectively) that also have the periodicity of amphipathic α helixes of a slightly different class, class G*.[12]

HDL discs are small unilamellar bilayers whose edges are surrounded by apoA-I.[13,14] Two general discoidal models have been proposed for apoA-I on the disc rim. (i) The "double belt" model, in which stacked monomers of apoA-I form continuous amphipathic α helixes parallel with the plane of the disc.[15] More recently, a modification of the double belt model, the "hairpin-belt", has been proposed in which apoA-I monomers form helical hairpins.[16,17] (ii) The "picket-fence" model, in which 22mer amphipathic α helical repeats of apoA-I form tandem antiparallel helixes perpendicular to the plane of the disc.[18] A 4 Å resolution solution phase X-ray structure for the lipid-associating domain of apoA-I supports the double belt model for discoidal HDL.[19] We recently proposed an atomic resolution double belt model for apoA-I associated with discoidal HDL.[20] Although the initial derivation of this model depended critically upon certain features of the X-ray structure, the entire model can be derived from first principles. The rigorous internal consistency of this detailed model and a number of subsequent physical chemical studies,[17,21–27] unequivocally support the double belt model (or the semi-equivalent hairpin-belt) rather than the picket fence.

The conformation of apoA-I is highly flexible, since apoA-I exists in different states: lipid-free, lipid-poor, and discoidal or spherical lipoproteins of different size. The size of discoidal complexes is determined primarily by the number of apoA-I molecules per particle, but analysis of reconstituted HDL discs formed between apoA-I and phospholipids has revealed several discrete sized particles in complexes containing a constant number of apoA-I per particle.[28] We proposed the hinged-domain hypothesis as a general mechanism to explain the size heterogeneity of dimyristoylphosphatidylcholine (DMPC):apoA-I discoidal complexes.[28] This hypothesis stated that one or more amphipathic α-helical segments of apoA-I undergo conformational changes to hinge off of or onto the disc edge. Since its original proposal, the general hypothesis has been supported by physical and chemical modification and immunochemical studies of apoA-I in reconstituted complexes of different lipid composition.[12] Many recent studies using limited proteolysis,[29,30] antibody binding,[31] and spectroscopic techniques,[32,33] and studies of lipoprotein particles containing two or four apoA-I molecules interacting with lipid vesicles labeled with photoactivable reagents[34] further support this hypothesis. However, no detailed molecular model to explain the hinged domain hypothesis had been proposed. Our objective in this work was to determine the molecular basis for the dynamic interaction of apoA-I with lipids that produces this variability in discoidal HDL particle size.

Results

Effects of the DMPC:apoA-I ratio on the size and distribution of discoidal complexes

Keeping the concentration of apoA-I constant, we prepared discoidal complexes with different concentrations of DMPC by the temperature-cycle procedure. Non-denaturing gradient gel electrophoresis (NDGGE) analyses of the complexes show

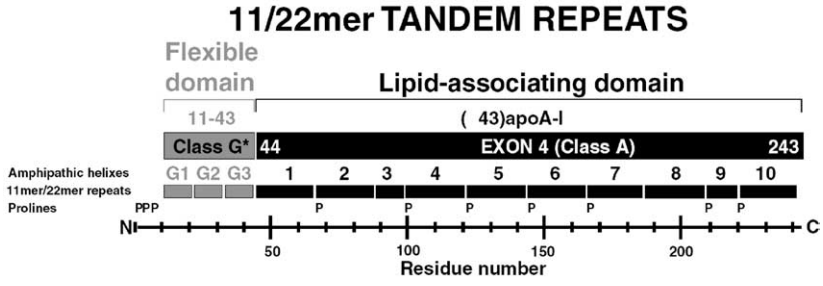

Figure 1. Domain structure of apoA-I. The tandem 11/22mer amphipathic α helical repeats in apoA-I are organized into two domains: a C-terminal lipid-associating domain made up of ten helical repeats and an N-terminal domain with significantly more flexible lipid association made up of three 11mer repeats.

that several defined discs are produced. Depending upon the conditions of disc formation, up to five different-sized discs are seen in the 95–120 Å Stokes diameter (S_d) range. This class of discs has been designated R2, referring to the presence of two apoA-I molecules on each particle as determined by chemical cross-linking (Figure 2). We have designated the first three discs R2-1, R2-2, and R2-3, in order of increasing size.

As shown in Figure 3(A), the R2-2 disc is generally the predominant particle when complexes are formed by temperature cycling; under the more equilibrated conditions of cholate dialysis, R2-2 is always present but becomes less prominent than the three larger R2 discs at or above a molar ratio of 150 : 1 (unless defined otherwise, the ratio refers to the molar ratio of DMPC to apoA-I) (Figure 4). Particle sizes, however, are independent of the method of particle formation. The size of the R2-2 particle increases from an S_d of 101.1(±1.7) Å ($n=6$) at a DMPC:apoA-I ratio of 25 : 1 to a S_d of 105.5(±0.7) Å ($n=6$) at a DMPC:apoA-I ratio of 600 : 1 ($n=6$). The R2-1 particle is more invariable in size with an S_d of 96.6(±1.6) Å ($n=36$), although the particle is slightly smaller and larger at its molar ratio limits of 25 : 1 ($S_d=94.9(\pm1.3)$ Å, $n=6$) and 150 : 1 ($S_d=97.9(\pm0.5)$ Å, $n=6$), respectively. This particle forms only at lower DMPC concentrations; at a molar ratio of 200 : 1 it disappears entirely.

The R2-3 particle is present in minimal to undetectable concentrations at lipid to protein molar ratios below 100 : 1; it becomes prominent at molar ratios of 150 : 1 and higher (Figure 3(A)). Like the R2-2 particle, the size of R2-3 increases with increasing molar ratios greater that 100 : 1, varying from an S_d of 107.4(±1.1) Å ($n=6$) at 150 : 1 to 109.5(±1.1) Å ($n=6$) at 600 : 1.

The R2-1 and R2-2 particles are remarkable, in that they vary little in size and relative concentrations at molar ratios of 100 : 1 and less. Within this range, a diminution in staining density of these two particles is associated with the appearance of free apoA-I, which increases in this concentration range in an inverse concentration dependency (Figure 3(B)). These results indicate that there is a minimum lipid:protein stoichiometry requirement for DMPC:AI complex formation, reflecting the fact that apoA-I appears insufficiently flexible in its association with DMPC to allow the formation of substantial amounts of discs with S_d less than 95 Å. A more detailed examination by NDGGE of the complexes formed in the molar ratios 100 : 1 to 150 : 1 (Figure 6(A)) shows no free apoA-I visible at the molar ratio of 110(±5) : 1 ($n=3$).

Effects of residues 1–43 of apoA-I on the size and distribution of discoidal complexes

We studied the effect of the flexible domain, residues 1–43, of apoA-I on size and distribution of discoidal complexes by NDGGE analysis of the complexes formed with full-length and with (Δ43)apoA-I. Complexes were formed by the cholate dialysis procedure at different lipid:protein ratios. The NDGGE analysis of the complexes (Figure 4, gel) shows that, as the DMPC:apoA-I

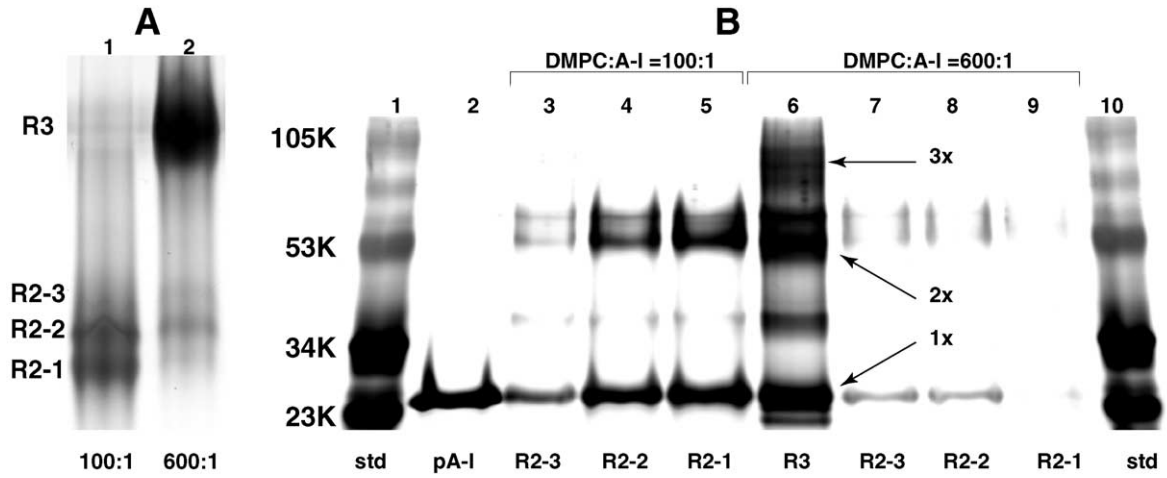

Figure 2. The apoA-I stoichiometry determined by chemical cross-linking of pre-formed DMPC:apoA-I discoidal complexes. Complexes were formed by incubating human plasma apoA-I at room temperature overnight with multilamellar DMPC at DMPC:apoA-I molar ratios of 100 : 1 and 600 : 1. Chemical cross-linking of apoA-I on the two different discoidal complexes in solution was then performed for one hour at room temperature with a 100-fold molar excess of Bis(sulfosuccinimidyl)suberate. (A) NDGGE of chemically cross-linked 100 : 1 and 600 : 1 DMPC:apoA-I molar ratio complexes in a 4–20% polyacrylamide gel. Gels were stained with colloidal blue. Lane 1, 100 : 1 complexes; lane 2, 600 : 1 complexes. (B) SDS-PAGE of apoA-I extracted from bands R2-1, R2-2, R2-3 and R3 of 100 : 1 and 600 : 1 complexes. Defined discoidal particles represented by bands labeled R2-1, R2-2, R2-3 and R3 in Figure 2(A) were cut out, minced and apoA-I extracted with SDS-PAGE sample buffer at room temperature. Gels were stained with silver. Lanes 1 and 10, MW standards (std); lane 2, uncrosslinked plasma apoA-I (pA-I); lanes 3 and 7, band R2-3 from 100 : 1 and 600 : 1 complexes, respectively; lanes 4 and 8, band R2-2 from 100 : 1 and 600 : 1 complexes, respectively; lanes 5 and 9, band R2-1 from 100 : 1 and 600 : 1 complexes, respectively; lane 6, band R3 from 600 : 1 complex. The positions of monomers (1x), dimers (2x) and trimers (3x) are indicated. The band between the monomer and the dimer may be a cross-linked folded (hairpin?) monomer.

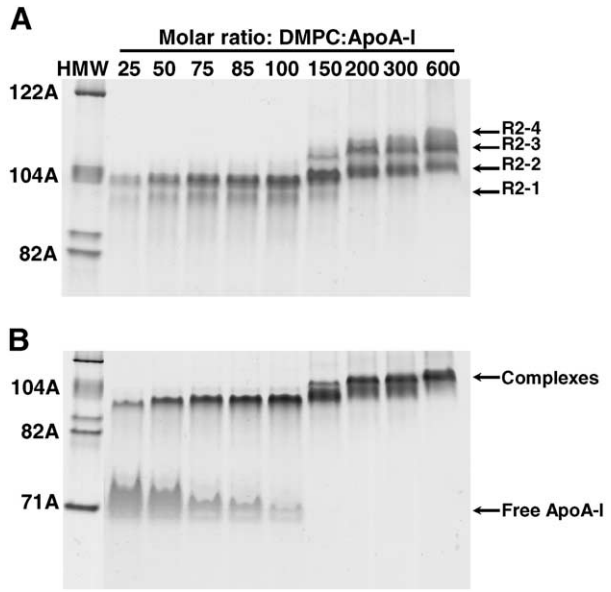

Figure 3. Effects of varying DMPC:apoA-I molar ratios on size and distribution of complexes formed by temperature cycling of multilamellar vesicles (MLV) of DMPC with apoA-I. Complexes were formed by incubating human plasma apoA-I with MLV in four cycles of 37 °C, 23 °C and 20 °C for one hour each at DMPC:apoA-I molar ratios of 25 : 1, 50 : 1, 75 : 1, 85 : 1, 100 : 1, 150 : 1, 200 : 1, 300 : 1 and 600 : 1. After cycling, the complexes were subjected to NDGGE analysis for 48 hours (A) (to obtain equilibrium Stokes diameters of complexes, upper panel) or six hours (B) (to observe the presence or absence of lipid-free apoA-I, lower panel) and stained with collodial blue. The Stokes diameter in Å of the high molecular mass standards in lane 1 (HMW) are indicated to the left of each band.

ratio increases, the sizes of R2-1 and R2-2 discs produced by both full-length and (Δ43)apoA-I approach common maxima: R2-1_{max} = 97.9 (±0.5) Å (n = 6) and 98.6(±0.9) Å (n = 3) for full-length and (Δ43)apoA-I, respectively, and R2-2_{max} = 105.5(±0.7) Å (n = 6) and 105.5 ± 0.6 Å (n = 3) for full-length and (Δ43)apoA-I, respectively. Of equal significance, the R2-3 discs, with R2-3_{max} of 110.7(±0.1) Å (n = 3), form only in complexes made with full-length apoA-I and not in those made with (Δ43)apoA-I (Figure 4, gel).

Not only does full-length apoA-I at molar ratios 150 : 1 or greater form R2-3 complexes when produced by cholate dialysis but it also forms two additional complexes larger than R2-3, termed R2-4 and R2-5 (Figure 4, gel), with maximum S_d = 114.4(±0.3) Å (n = 3) and 120.5(±0.2) Å (n = 3), respectively. Careful inspection of Figure 3(A) shows that R2-4 and R2-5 also appear to be formed when DMPC:apoA-I discs are created using the temperature-cycling technique but are difficult to distinguish because they are not well separated from R2-3.

There is, however, one clear difference between the R2-1 and R2-2 discoidal complexes produced by full length *versus* (Δ43)apoA-I. The R2-2 disc is the predominant apoA-I complex produced by full-length apoA-I at lower DMPC:apoA-I ratios, e.g. at 100 : 1 (Figure 3(A)). On the other hand, the R2-1 disc is the predominant dimer complex produced by (Δ43)apoA-I at molar ratios of 100 : 1 or lower (Figure 4, gel and Figure 6(B)); the R2-1 disc is even more prominent compared to the R2-2 disc when complexes are produced by temperature cycling (Figure 8). This shows that, while the N-terminal 43 residues of apoA-I have no measurable effect on maximal size of the R2-1 and R2-2 discs, this flexible domain of apoA-I affects the relative distribution of the two discs. Thus, the maximum S_d of the two smaller DMPC:apoA-I complexes, R2-1 and R2-2, are independent of the N-terminal 43 residues (the flexible domain) of apoA-I, while the flexible domain is absolutely required for the formation of the three larger complexes, R2-3, R2-4 and R2-5. Further, R2-1 and R2-2 maintain minimal Stokes diameters even at the lower lipid:protein molar ratios (below 100 : 1), leaving the excess apoA-I as lipid-free.

On the basis of these results, the conformation of apoA-I on the R2-2 disc can be modeled most simply (Figure 4, second model counterclockwise from left) as an amphipathic helical double belt extending, on average, the full length of the lipid-associating domain with N and C-terminal ends in direct contact (measured S_d max = 105.5 Å; calculated model diameter = 105.5 Å). The smallest of the discs, R2-1, then models (Figure 4, first model counterclockwise from left) as the R2-2 conformation with a major portion of an antiparallel segment of two adjacent 22mer helixes hinged off the disc edge (measured S_d max = 98 Å; calculated model diameter assuming hinging of a complete 22mer helix = 95 Å).

Finally, the conformations of full-length apoA-I on the flexible domain-dependent discs (R2-3, R2-4 and R2-5) model (Figure 4, third, fourth and fifth models counterclockwise from left, respectively) as the R2-2 conformation extended on the disc edge by one (measured S_d max = 110 Å; calculated model diameter = 111 Å), two (measured S_d max = 114 Å; calculated model diameter = 116 Å) or three (measured S_d max = 121 Å, calculated model diameter = 121 Å) of the 11 residue tandem amphipathic helical repeats, respectively, contained within the flexible domain (termed G1, G2 and G3, see Figure 1).

As a test of our model for discoidal HDL size heterogeneity illustrated schematically in Figure 4, we hypothesized that addition of residues 1–43 to (Δ43)apoA-I:DMPC complexes might allow (Δ43)apoA-I to form the 1–43-dependent discs, R2-3, R2-4 and R2-5. As a first step in testing this hypothesis, we analyzed the affinity of a synthetic peptide analog of residues 1–43, N43, for DMPC. The peptide N43 was subjected to cholate dialysis at a DMPC:peptide molar ratio of 100 : 14 and NDGGE performed. Under these conditions, a broad bimodal band representing a peptide:DMPC

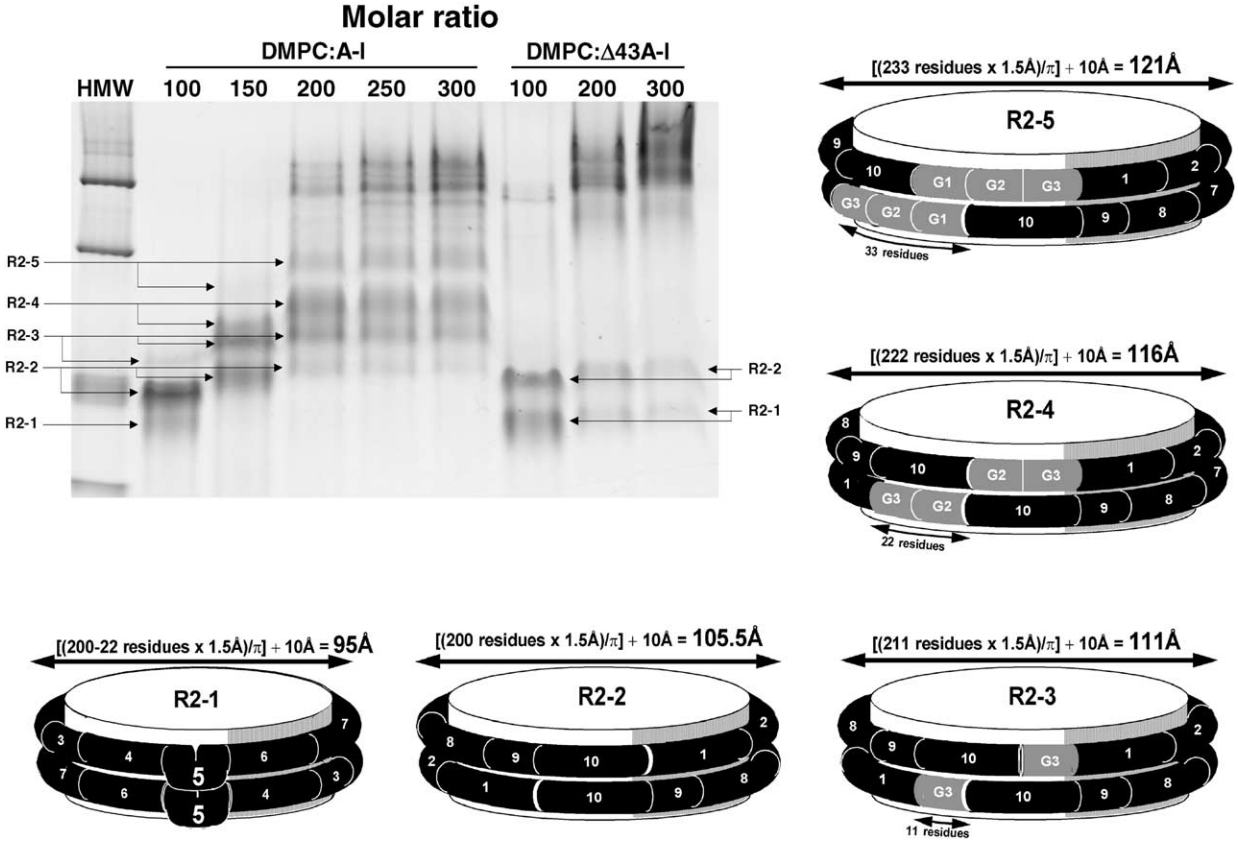

Figure 4. Analysis of size and distribution of discoidal complexes formed by full-length *versus* (Δ43)apoA-I after cholate dialysis at varying DMPC:protein ratios and illustration of schematic models developed to explain the observed particle sizes. Gel. NDGGE analysis in a 4–20% polyacrylamide gel of discoidal complexes formed by incubating DMPC with full-length apoA-I at molar ratios of 100 : 1, 150 : 1, 200 : 1, 250 : 1 and 300 : 1 and with (Δ43)apoA-I at molar ratios of 100 : 1, 200 : 1 and 300 : 1. Complexes were formed by the cholate dialysis method and subjected to NDGGE analysis. The positions of five distinct discoidal complexes, R2-1, R2-2, R2-3, R2-4 and R2-5, containing two apoA-I per disc are indicated by arrows. In general, the Stokes diameter of each particle increases with lipid concentration up to a limiting value. Models, schematics of DMPC:apoA-I disc models for R2-1 through R2-5 based upon the LL5/5 double belt rotamer conformation.[20] The calculations shown above each disc schematic assume an α-helical rise of 1.5 Å per residue and an α helix center to edge distance of 5 Å.[19]

complex was observed with S_d of approximately 200 Å and 170 Å (data not shown), presumably vesicles and discs, respectively (David Atkinson, personal communication). We further confirmed the lipid-associating ability of N43 by taking advantage of the presence of a single Trp residue in N43. Emission spectra of N43 and the DMPC:N43 complex showed that N43 shows a blue shift in the Trp emission maximum (em max 332 nm) and an increase in the emission intensity in the DMPC:N43 complex compared to N43 in buffer (em max 350 nm) (data not shown), indicating the incorporation of the Trp residue in the hydrophobic environment of the DMPC bilayer. In addition, a comparison of acrylamide quenching in PBS with that in the DMPC bilayer reveals that the Trp residue in N43 is shielded in the presence of lipid compared to that in PBS (data not shown), further indicating that the N43 peptide is associated with the DMPC bilayer.

We then performed experiments to test our hypothesis that addition of residues 1–43 to DMPC:(Δ43)apoA-I complexes would allow (Δ43)apoA-I to form the 1–43-dependent discs, R2-3, R2-4 and R2-5. Complexes of DMPC and (Δ43)apoA-I were formed by cholate dialysis at a molar ratio of 300 : 1 in the presence of N43 at a 1 : 1 molar ratio with (Δ43)apoA-I or in its absence. Additionally, half of the complex formed in the absence of N43 was subsequently incubated overnight with N43 at a 1 : 1 molar ratio with (Δ43)apoA-I, and all three preparations were subjected to NDGGE. Examination of the scan of the gel shown in Figure 5(A) shows clearly that the 1–43-dependent complex R2-3, and perhaps R2-4, is produced by the presence of N43 whether present during complex formation or added after complex formation, while the complex produced without N43 shows essentially no R2-3.

To further confirm the absence of R2-3 when N43 is not present, complexes were made with (Δ43)apoA-I in the absence of N43 at two molar ratios, 100 : 1 and 300 : 1, and the resultant NDGGE gels scanned (Figure 5(B)); no evidence for R2-3 can be detected.

Finally, we used ^{125}I-labeled N43 to confirm the

results of Figure 5(A). Complexes of DMPC:(Δ43) apoA-I and DMPC:apoA-I at 100 : 1 and 150 : 1 molar ratios were made by cholate dialysis in the presence and absence of equal molar concentrations of [^{125}I]N43, NDGGE was performed, the gels were stained with colloidal blue, sliced at 0.5 cm intervals and individual slices counted. From Figure 5(C) and (D), complexes made with full-length apoA-I at 100 : 1 and 150 : 1 molar ratios show little, if any, association with [^{125}I]N43. In contrast, complexes made with (Δ43)apoA-I at either molar ratio show some association with [^{125}I]N43. The 150 : 1 complexes are expected to form significantly more R2-3 than the 100 : 1 complexes and, in line with this expectation, the 150 : 1 complex (Figure 5(D), upper panel) shows more association with [^{125}I]N43 than does the 100 : 1 complex (Figure 5(C), upper panel). At 150 : 1 (Figure 5(D)), R2-3 can be detected readily by gel scanning, and slice 7, corresponding to the position of R2-3, contains approximately 3% of all counts applied to the gel; the R2-3 peak seen in the scan contains approximately 3% of the total protein on the gel as determined by densitometric analysis. These results indicate that R2-3 formed by

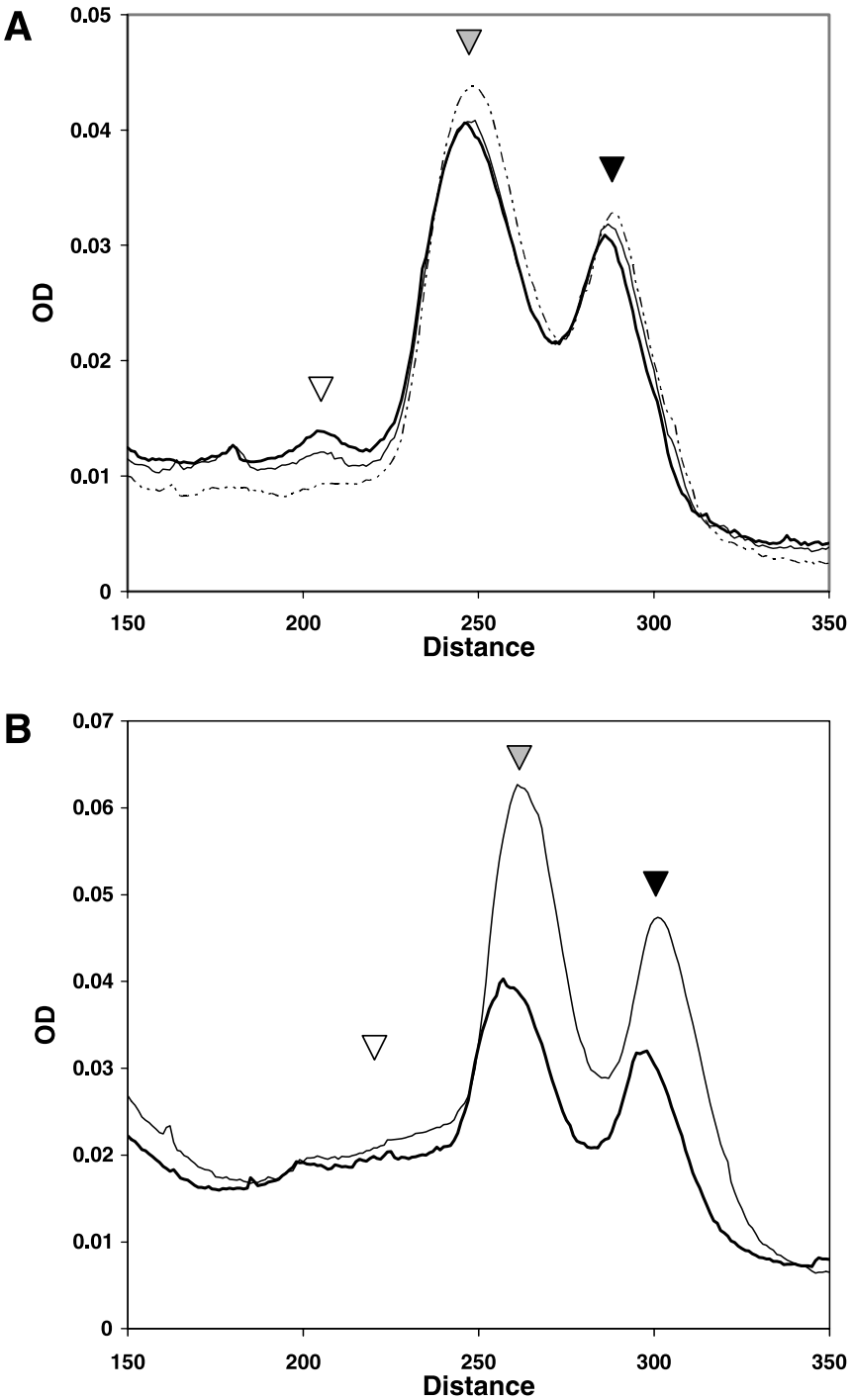

Figure 5 (*legend opposite*)

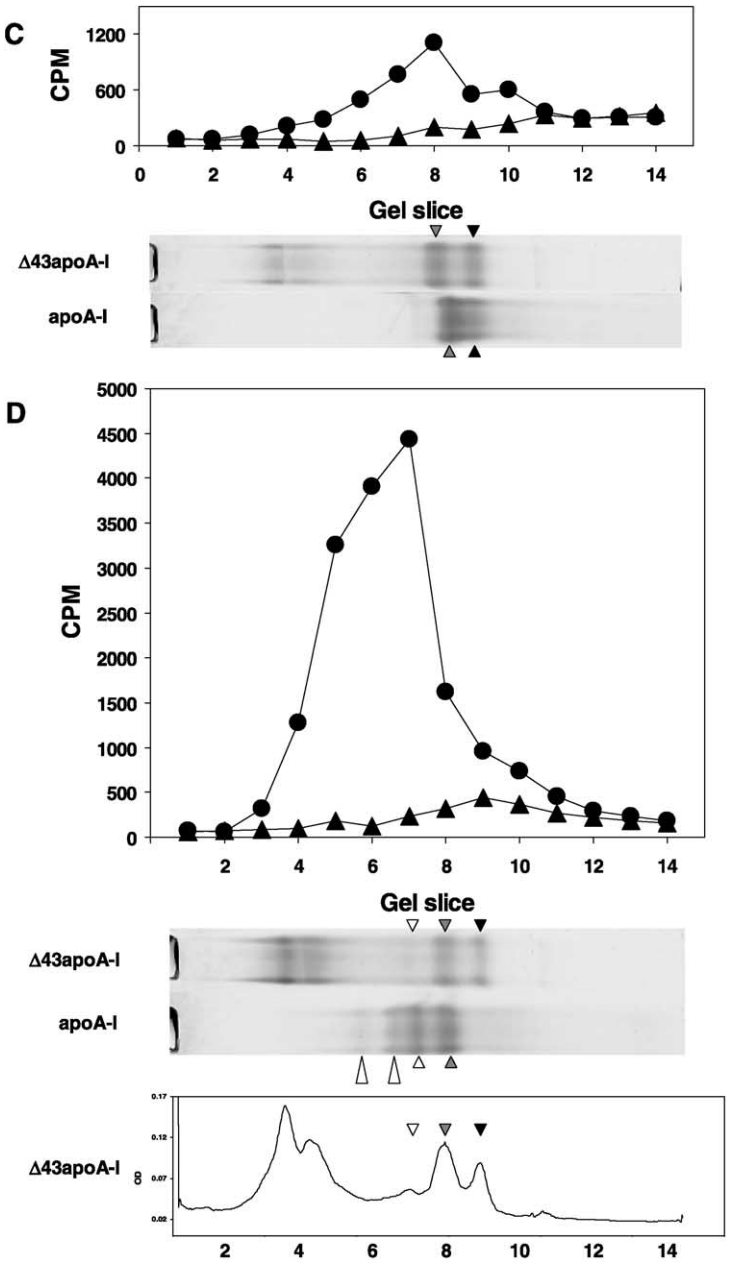

Figure 5. Effects of adding the N43 peptide on the size and distribution of discoidal complexes. (A) Densitometric scan of NDGGE gels of complexes formed with DMPC and (Δ43)apoA-I by cholate dialysis at a molar ratio of 300 : 1 in the presence (thick continuous line) or absence (dotted line) of N43 at a 1 : 1 molar ratio with (Δ43)apoA-I. Or, the complex formed in the absence of N43 was subsequently incubated overnight with N43 at a 1 : 1 molar ratio with (Δ43)apoA-I (thin continuous line). The positions of R2-3, R2-2, and R2-1particels are indicated by an open, shaded, and filled arrowhead, respectively. The 1–43-dependent complex R2-3 (open arrowhead) is produced by the presence of N43 whether present during complex formation (thick continuous line) or added after complex formation (thin continuous line), while the complex produced without N43 shows essentially no R2-3 (dotted line). (B) Densitometric scan of NDGGE gels of complexes formed with DMPC:(Δ43)apoA-I in the absence of N43 at two molar ratios, 100 : 1 and 300 : 1. No evidence for R2-3 (open arrowhead) can be detected, further confirming the absence of R2-3 when N43 is not present. (C) NDGGE and radioactivity in continuous gel slices of complexes of DMPC:(Δ43)apoA-I (●) and DMPC:apoA-I (▲) at 100 : 1 molar ratios made by cholate dialysis in the presence of equal molar concentrations of [^{125}I]N43. The R2-1 and R2-2 particles on the gel (stained with colloidal blue) are indicated by continuous and shaded arrowheads, respectively. Radioactivity determination of the gel shows some association of [^{125}I]N43 with the R2-2 particle formed with (Δ43)apoA-I (●) but no association of [^{125}I]N43 with complexes formed with full-length apoA-I (▲). (D) NDGGE and radioactivity in continuous gel slices of complexes of DMPC:(Δ43)apoA-I (●) and DMPC:apoA-I (▲) at 150 : 1 molar ratios made by cholate dialysis in the presence of equal molar concentrations of [^{125}I]N43. The 150 : 1 complexes form significantly more R2-3 than the 100 : 1 complexes as indicated by a small open arrowhead on the gel. The positions of R2-4 and R2-5 particles are indicated by large open arrowheads. Radioactivity determination of the gel (upper panel) shows that the 150 : 1 complexes of DMPC:(Δ43)apoA-I have more association with [^{125}I]N43 (●), whereas little, if any, [^{125}I]N43 is associated with complexes formed with full-length apoA-I (▲). The densitometric scan (lower panel) of the gel with DMPC:(Δ43)apoA-I complexes readily detects R2-3 particle (a peak indicated by an open arrowhead).

coincubating [^{125}I]N43 and (Δ43)apoA-I contains about 1 mol of N43 for each 1 mol of (Δ43)apoA-I. The broadness of the radiolabel peak (Figure 5(D), upper panel) suggests that R2-4 and R2-5 are formed also but at lower concentrations than R2-3.

Circular dichroism (CD) spectroscopy of complexes formed by incubating DMPC with full-length and (Δ43)apoA-I

NDGGE was used to examine changes in distribution of the R2-1, R2-2, R2-3 and R2-4 particles and the presence or absence of free apoA-I in complexes made with full-length and (Δ43)apoA-I over a narrower concentration range than that of Figures 3 and 4. The results are shown in Figure 6. It is of importance for physical chemical studies by CD spectroscopy that complexes of full-length apoA-I made at the molar ratio of 100 : 1 by cholate dialysis (Figure 6(A)) contain mostly R2-2 and vanishingly small amounts of free apoA-I; at 110 : 1 no free apoA-I can be identified. Further, when complexes are made at 150 : 1, the predominant particles formed are R2-3 and R2-4, the R2-2 particle is minor and R2-1 is non-existent.

Of equal importance for studies by CD spectroscopy, complexes of (Δ43)apoA-I made at the molar ratio of 50 : 1 by cholate dialysis (Figure 6(B)) contain only the R2-1 particle and very little free (Δ43)apoA-I; at 60 : 1 no free (Δ43)apoA-I can be identified. Complexes made at 100 : 1 contain predominantly R2-1 particles with some R2-2.

CD spectroscopic comparisons of lipid-free protein and discoidal complexes formed by full-length and (Δ43)apoA-I were then used to examine possible protein structural differences between the different R2 complexes. The models developed in Figure 4 suggest that formation of R2-3, R2-4 and R2-5 involves the sequential addition of 11 residue α-helical tandem repeats of the flexible domain to the disc edge. Because of the strong effects of lipid association on the α helicity of apoA-I, a reasonable possibility would be that increasing concentrations of R2-3, R2-4 and R2-5 relative to R2-2 might result in increasing overall α helicity. The results shown in Figure 7 and Table 1 support this possibility. As the molar ratio of the discoidal complex of DMPC with full-length apoA-I increases from 100 : 1 to 150 : 1, the α helicity increases from 74% to 83%, compatible with the conversion from a complex containing mostly R2-2 to one containing mostly R2-3 and R2-4. These results suggest that the helicity increase for full-length apoA-I with increasing lipid concentration is related to sequential insertion of helical domains from the flexible domain, absent from (Δ43)apoA-I, onto the growing disc edge. Finally, the minimal change in percentage helicity as the molar ratio of DMPC to (Δ43)apoA-I increases from 50 : 1 to 100 : 1 suggests that the hinged domain remains mostly helical as it hinges off the disc edge in R2-1.

Kinetics of disc formation

To examine whether lipid transfer might be involved in the kinetics of *in vitro* disc formation, we asked whether preformed discs would take up additional DMPC when incubated at 23 °C with bulk DMPC in the form of multilamellar vesicles. As shown in Figure 8, we found that preformed discs made from either apoA-I or (Δ43)apoA-I took up essentially all of the free DMPC to form complexes identical with those made *de novo* at the same DMPC:protein ratio. For example, preformed discs made with either apoA-I or (Δ43)apoA-I at a 100 : 1 DMPC:protein molar ratio when incubated with sufficient bulk DMPC to create a final molar ratio of 200 : 1 formed the

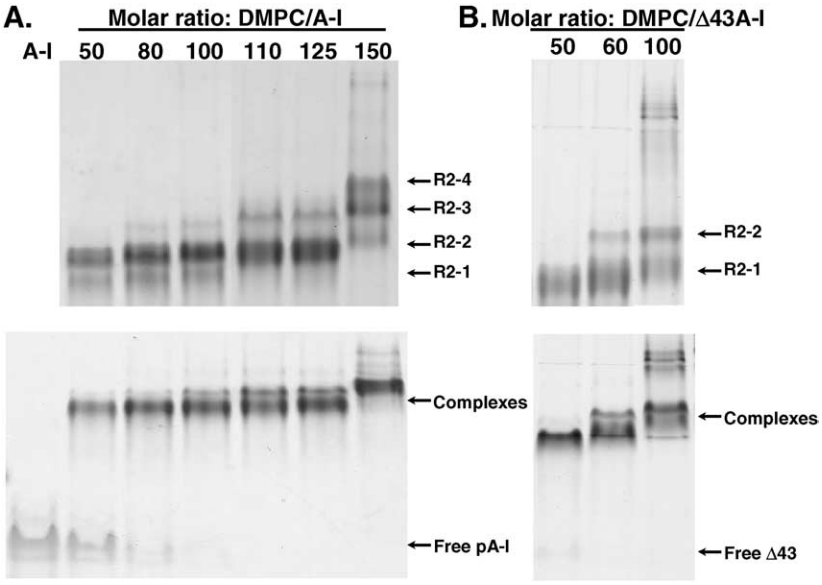

Figure 6. Analysis of size and distribution of complexes formed by full-length *versus* (Δ43)apoA-I within a narrow range of DMPC:protein ratios. The complexes were prepared by the cholate dialysis method. (A) NDGGE of complexes formed by full-length apoA-I. Complexes at the molar ratio of 100 : 1 contain mostly R2-2 (upper panel) and vanishingly small amounts of free apoA-I (lower panel); at 110 : 1 no free apoA-I can be identified (lower panel). Complexes made at 150 : 1 (upper panel) contain predominantly R2-3 and R2-4 with little R2-2 and no R2-1. (B) NDGGE of complexes formed by (Δ43)apoA-I. Complexes of (Δ43)apoA-I made at the molar ratio of 50 : 1 contain only the R2-1 particle (upper panel) and very little free (Δ43)apoA-I (lower panel); at 60 : 1 no free (Δ43)apoA-I can be detected (lower panel). Complexes made at 100 : 1 contain predominantly R2-1 particles with some R2-2.

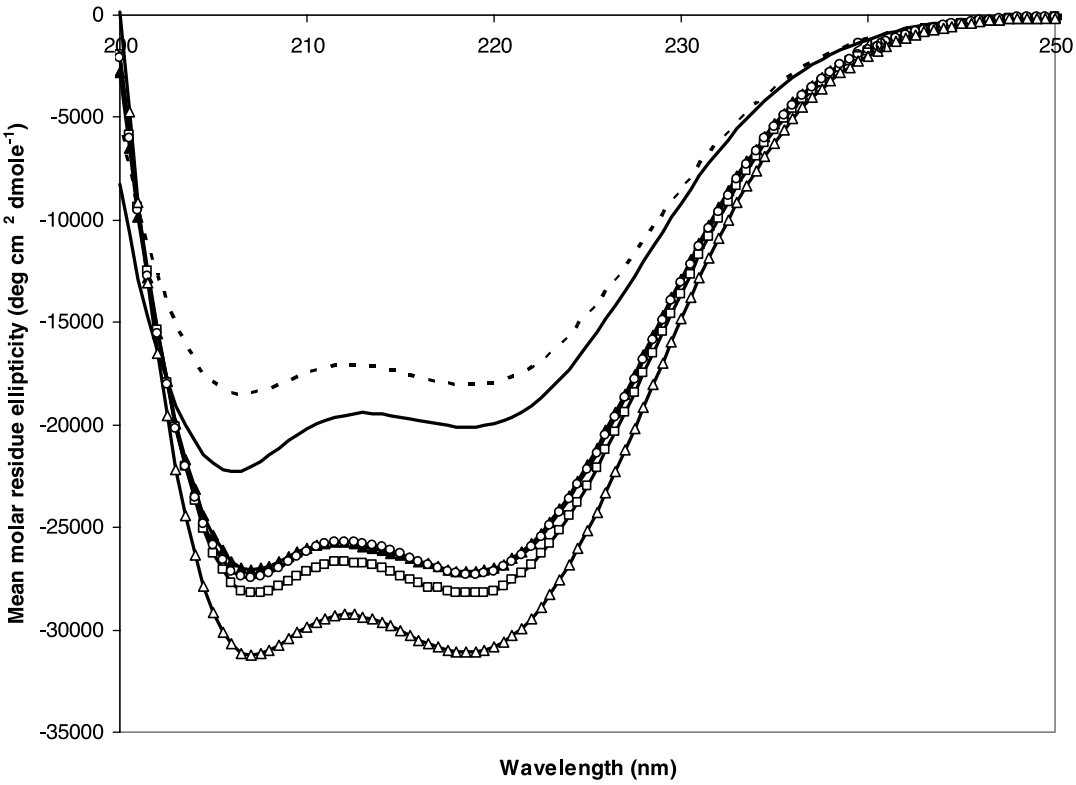

Figure 7. Circular dichroism spectra of lipid-free proteins and DMPC complexes of full-length and (Δ43)apoA-I formed by the cholate dialysis method. Spectra shown are data averaged from three independent experiments for lipid-free apoA-I (–), lipid-free (Δ43)apoA-I (- - -), 50 : 1 DMPC:(Δ43)apoA-I complexes (▲), 100 : 1 DMPC:apoA-I complexes (○), 100 : 1 DMPC: (Δ43)apoA-I complexes (□), and 150 : 1 DMPC:apoA-I complexes (△).

Table 1. Circular dichroism spectroscopy of DMPC complexes of full-length and (Δ43)apoA-I

Apolipoprotein	α Helicity (%)			
	Protein in solution	DMPC:protein complexes (M:M)		
		50 : 1	100 : 1	150 : 1
apoA-I	57	–	74	83
(Δ43)apoA-I	52	74	76	–

same NDGGE pattern as discs made *de novo* at a starting molar ratio of 200 : 1. These results support the concept that *in vitro* disc formation by the cycle procedure involves DMPC transfer from the bulk phase to nascent discs.

Possible role of helix 5 in the size and distribution of discoidal HDL complexes

The model for the smallest apoA-I lipid complex, R2-1, requires that a portion of the lipid-associating domain of apoA-I hinge away from the disc edge. In the simplest approximation, the hinge region should be the region of lowest lipid affinity. One approach to delineating the overall lipid-associating properties of apoA-I is to study the lipid-associating properties of individual and overlapping tandem amphipathic helical domains of this apolipoprotein. To achieve this goal, we studied an extensive set of synthetic peptide analogs of apoA-I.[35,36] Figure 9(A) represents a graphic summary of these studies. This Figure clearly indicates that lipid affinity is greatest at the N and C-terminal ends of the sequence encoded by exon 4, residues 44–241, results supported by site-directed mutagenesis studies from other laboratories.[37–39] It is of interest regarding the location of the hinge region that Figure 9(A) shows a U-shaped lipid affinity curve for the lipid-associating domain of apoA-I, with the low point in lipid affinity occurring at helix 5.

Phylogenetic studies suggest that helix 5 is structurally unique and may be metastable. In all mammalian apoA-I sequences, helix 5 is a continuous amphipathic α helix, but in apoA-I sequences of birds and fish, LOCATE analysis predicts that helix 5 represents two amphipathic α helixes (Figure 9(B)). This suggests that the hairpin-belt conformer may be evolutionarily ancient, with helix 5 forming the hairpin, while the double belt conformer is a more recent evolutionary adaptation.

The helix 5–helix 5 pair in both the 129j rotamer[20] and the X-ray structure[19] creates a charge:charge apposition of residue K133 from each helix. This is of importance, because K133 is in the deep position 2 in the α11/3 helical pinwheel (see Discussion). Residue K133 is conserved in all mammals and birds (data not shown). In the X-ray structure for residues 44–243 of apoA-I,[19] the helix 5–helix 5

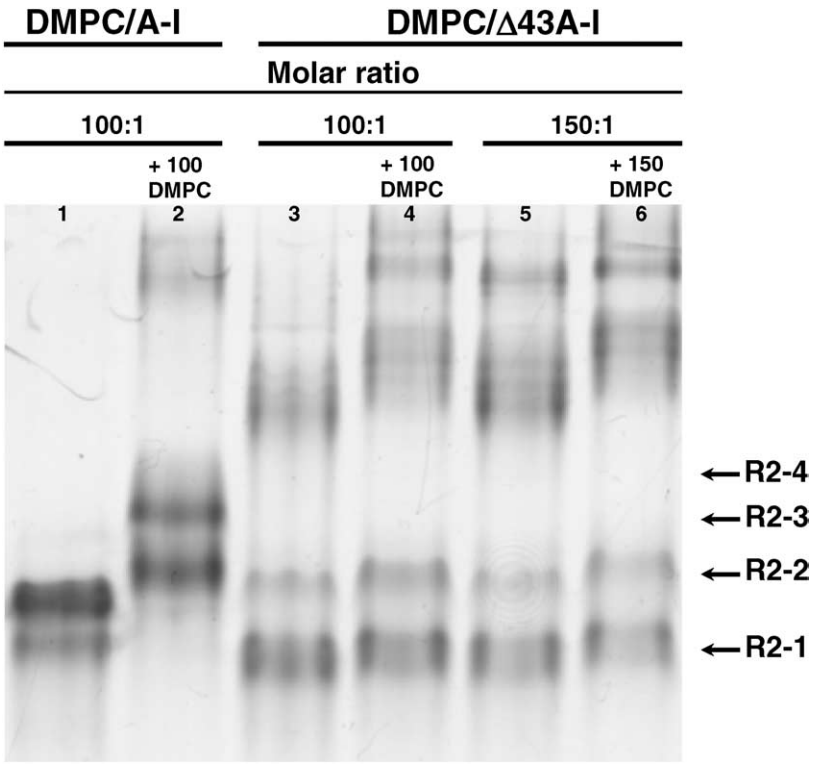

Figure 8. Kinetic analysis of disc formation. DMPC:apoA-I and DMPC: (Δ43)apoA-I were formed by the temperature-cycle method at the molar ratio of 100 : 1 (lane 1 and 3) or 150 : 1 (lane 5). Half of the preformed complexes were then incubated with additional 100 or 150-fold molar excess of DMPC MLVs to reach final lipid:protein ratio of 200 : 1 (lane 2 and 4) or 300 : 1 (lane 6). All complexes were subjected to NDGGE.

antiparallel pair (Figure 9(C)) assumes a "mouth"-like shape, tightly packed at the ends (center to center distance = 10 Å) and separated centrally (center to center distance = 13 Å).

Finally, our previously published molecular dynamics (MD) simulation of the 129j rotamer sheds possible light on the location of the hinged domain.[40] Figure 9(D) represents a snapshot of the helix 5–helix 5 region after 600 ps of simulation. Note that, at this point in the simulation, there is an opening of a mouth between the helix5–helix 5 antiparallel pair exposing the underlying fatty acyl chains.[40] This mouth seems to open and close during the 1 ns simulation. No other region of the 129j rotamer structure exposes this much lipid hydrocarbon during any time-point in the 1 ns simulation. Note from the upper part of the figure that the K133 charges in juxtaposition appear to have repelled each other, contributing to the opening of the mouth.

Discussion

Working model of the molecular basis for size heterogeneity of apoA-I discoidal particles

Our models assume a double belt structure.[20] The atomic details of the double belt model followed *a priori* from the starting assumption that lipid imposes profound constraints on the conformation and orientation of lipid-associated proteins.[12] The model was derived entirely from three simple conformational constraints: (i) the amphipathic α helix as the major lipid-associating motif of apoA-I;[9,13,16,20] (ii) planar discoidal HDL geometry;[1,5,17,28] and (iii) curvature dictated by the boundary between the low dielectric lipid and the high dielectric solvent,[41] each of which is supported by abundant experimental evidence. In the resulting model, two apoA-I molecules were wrapped beltwise around a small discoidal patch of bilayer containing 160 lipid molecules. Each apoA-I monomer formed a curved, planar amphipathic α-helical ring with 11/3 (approximately 3.67) residues per turn (termed an α11/3 helix) in which the hydrophobic surface faced inward toward the lipid disc. Two types of possible salt-bridges between pairwise apoA-I belts were observed using the computer program, ALIGN: deep and superficial.[20] The deep (2-2) salt-bridges are significantly more deeply buried on the convex or inner lipid-associating edge of the helical rings and thus are presumably energetically more favorable than the superficial (9-5) salt-bridges.

Although the α11/3 helix, as a distinct type of helix, is not a proven concept, several lines of evidence suggest its existence. (i) The α11/3 helix was mentioned by Linus Pauling in his original description of the α helix when he observed that the pitch of the α helix could vary from 3.6 (18/5) to 11/3 (3.67) residues per turn without significant energy penalty.[42] (ii) The 11 residue tandem periodicity, the 11 residue salt-bridge periodicity, and the straightening of the polar/hydrophobic edges of the entirety of helixes 2–9, a span of 154 residues of apoA-I strongly suggest the existence of an 11/3 periodicity in apoA-I.[20] This periodicity occurs also in apoA-IV, a much longer apolipoprotein (unpublished observations). (iii) Finally, recent publications suggest that amphipathic α11/3 helixes are a common feature in other proteins,

such as α-synuclein, that contain lipid-associating amphipathic helixes.[43,44]

Although the models in Figures 4 and 10 show the portions of apoA-I associated with the disc edge as completely helical, this is purely schematic. We are not implying that the double belts are static α-helical structures. The models in Figures 4 and 10 are a first approximation of a much more dynamic particle. The molecular model of Figure 9(D), representing a molecular dynamic snapshot, is more representative

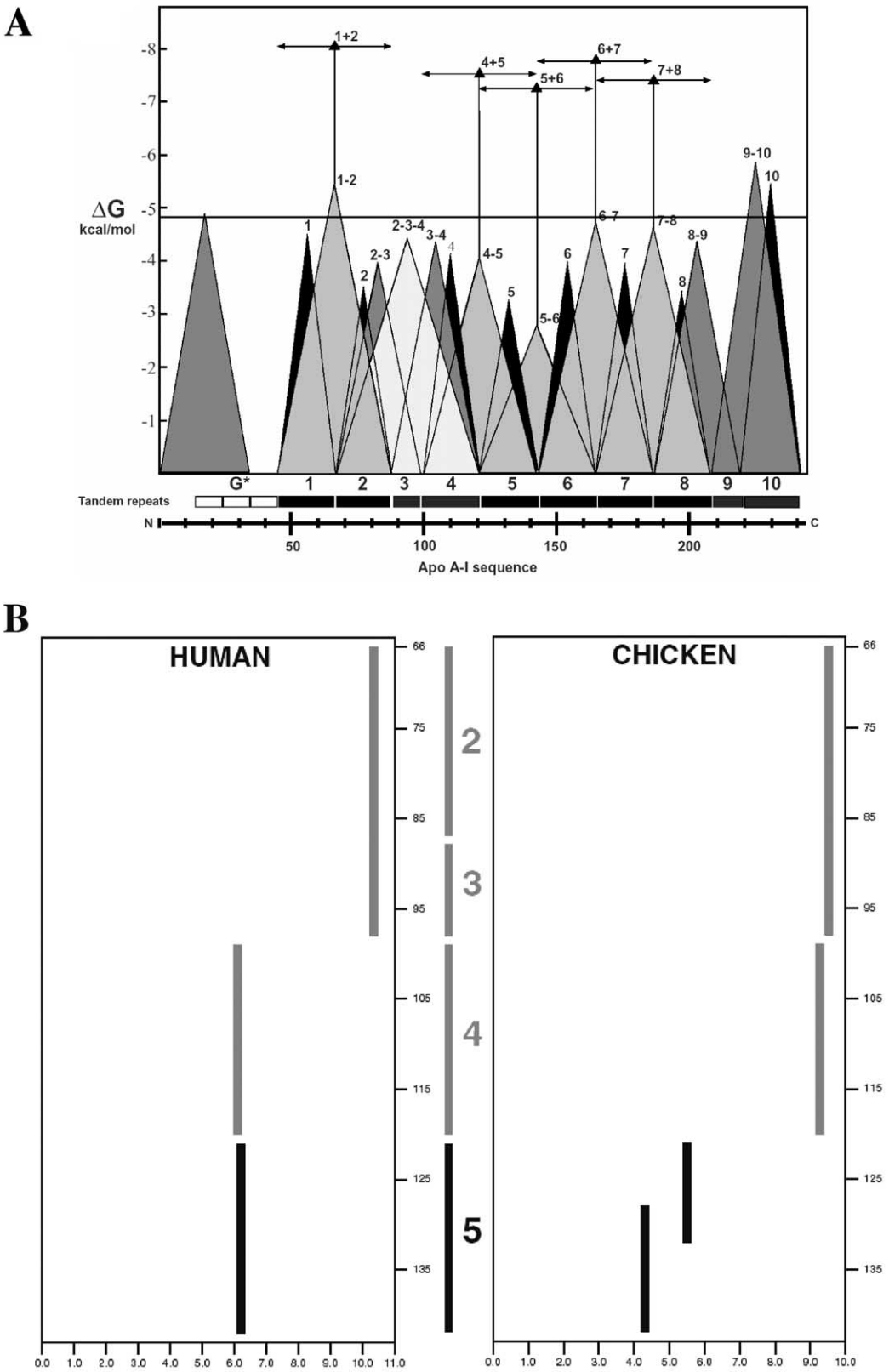

Figure 9 (*legend p.1304*)

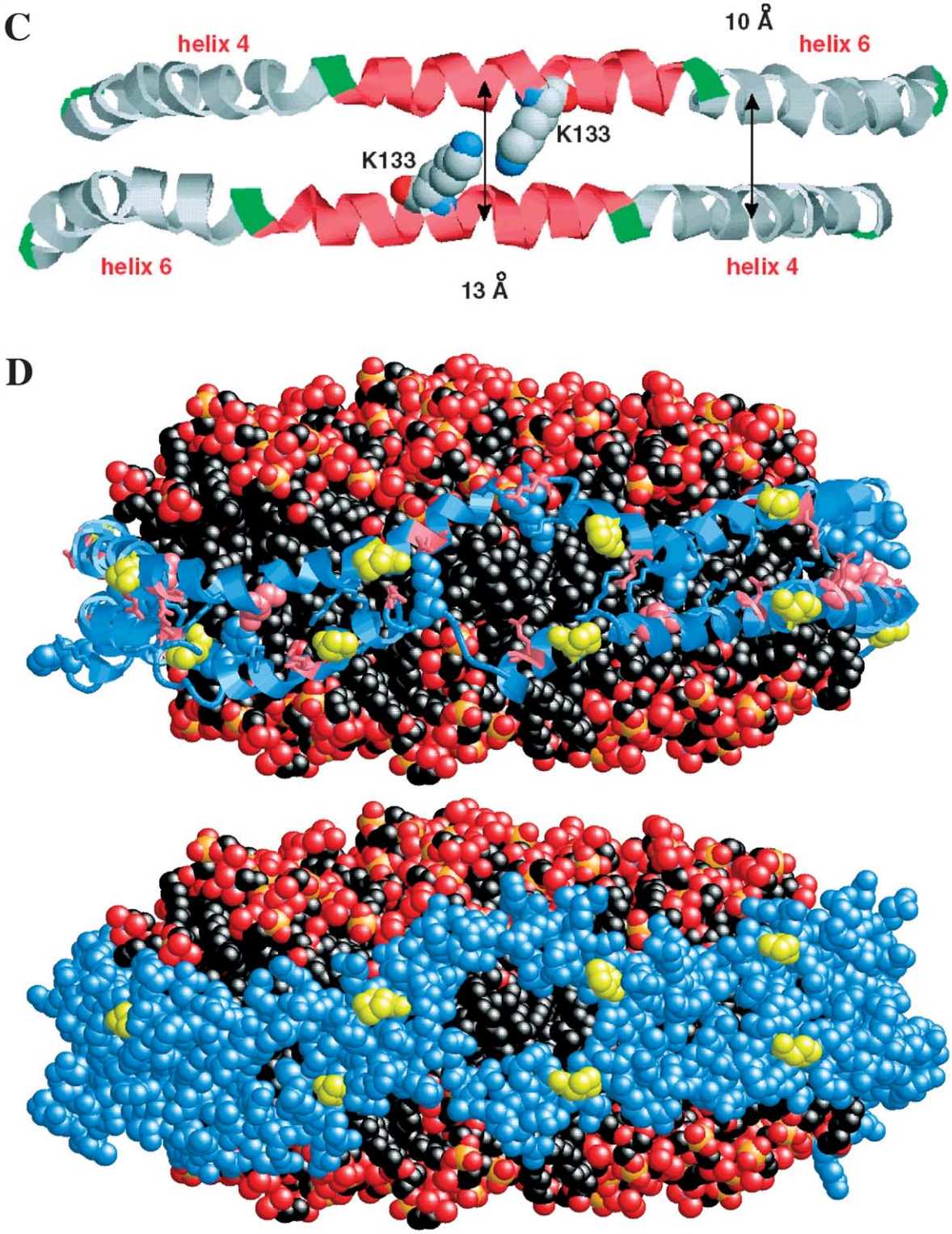

Figure 9. Properties of helix 5. (A) Plot of the experimentally derived free energy of lipid-association (with MLV) for synthetic peptide homologs of single and multiple tandem repeating units of human apo A-I. The *x*-axis, residue position and position of tandem helical repeats; the *y*-axis, experimentally measured free energy of lipid-association for each peptide.[35,61] Experimental results for each peptide are represented by a large triangle: the apex plots the measured free energy of lipid-association and the base indicates the peptide position in the apo A-I amino acid sequence. The darker the shading of the triangle, the smaller the peptide. Peptide lengths are 22, 33, 44 and 55 residues. The small filled triangles bisected by horizontal double-headed arrows indicate the expected free energy of lipid-association for 44mers if the free energy of individual 22mers summed in a linear fashion. The horizontal line the length of the Figure at approximately 5 kcal/mol is the experimentally determined free energy of lipid-association of native apo A-I with MLV. (B) Two-dimensional αLOCATE analysis of residues 66–141 (helixes 2–5) of apoA-I from human and chicken. Filled bars within boxes represent individual amphipathic α helixes identified by the αLOCATE algorithm; the *x*-axis of boxes,

of the expected apoA-I ring structure than Figures 4 and 10.

However, we would like to point out that Figure 9(D) is itself a static snapshot of a molecular dynamic simulation. Molecular dynamic simulations in our hands to date show dynamic changes in the helicity of all apoA-I segments. In molecular dynamic simulations of R2-2 under starting conditions, we have yet to observe a single segment of the apoA-I associated with the disc edge that is always non-helical. A fixed non-helical segment in the R2-2 model, for example, would be energetically unfavorable, since it would not provide adequate lipid coverage and would expose unformed backbone hydrogen bonds to a low dielectric environment. We suggest, rather, that there is a kinetic or dynamic distribution of helical and non-helical segments sampled over time. Certain regions associated with the disc edge will have a greater tendency to be helical than others but not in an all-or-none fashion. Thus, because of the dynamic nature of an α helix, especially one associated with lipid, the α11/3 helix, rather than being a fixed structure, represents more of an ideal construct, one that allows development of starting models for molecular dynamics simulations.

As we show clearly in the data presented here, discs containing two apoA-I molecules, the R2 complexes, display two types of size heterogeneity (Figures 3 and 4). (i) The most obvious form of size heterogeneity is the quantification of discs into five distinct, fairly monodisperse particles, termed step-wise heterogeneity. (ii) The more subtle form of size heterogeneity is a seemingly smooth increase in size of each of the individual particles with increasing DMPC:apoA-I molar ratios, termed continuous heterogeneity.

A number of years ago we proposed the hinged-domain hypothesis as a general mechanism to explain the step-wise size heterogeneity of DMPC:apoA-I discoidal complexes.[28] This hypothesis stated that one or more amphipathic α-helical segments of apoA-I undergo conformational changes to hinge off of or onto the disc edge. Although many physical, chemical, and biological studies have supported this hypothesis since its original proposal,[12,29–34] no detailed molecular model of the hinged domain had been proposed until now.

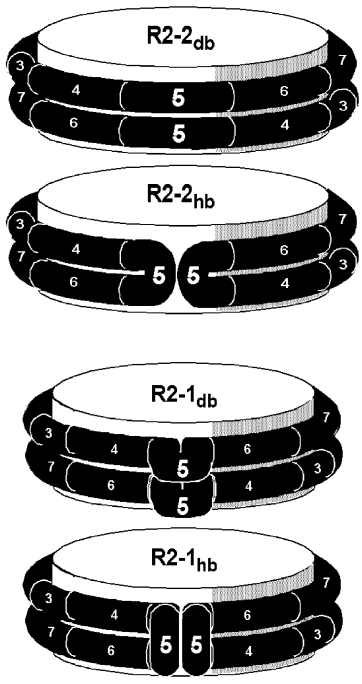

Figure 10. Schematic presentation of helix 5–helix 5 interactions in the double belt (db) and hairpin-belt (hb) models for R2-2 and R2-1. Upper two panels: R2-2 complexes in the double belt or head to head hairpin-belt model, respectively, showing the helix 5–helix 5 contact. Lower two panels: R2-1 complexes in the double belt or head to head hairpin-belt model, respectively, showing the hinged domains involving helix 5.

The current study provides a simple but detailed and internally consistent model to explain step-wise size heterogeneity. The experimental underpinning of the model is the generally accepted assumption that Stokes diameters of discoidal objects measured by NDGGE are accurate measures of the diameters of the discs. Therefore, the fact that the R2-1 and R2-2 discs formed by both full-length and (Δ43)apoA-I have identical Stokes diameters

calculated lipid affinity (Λα); the *y*-axis of boxes, residue number. The central bars indicate the position of 11mer/22mer helical repeats. Amphipathic α helixes from helix 5 are in black. All other amphipathic α helixes are in gray. (C) Molecular graphics model created with RASMOL[62] showing the "mouth"-like shape of the helix 5–helix 5 interface in the X-ray crystal structure of apoΔ43A-I.[19] Residues 99–165 (helixes 4–6) are displayed in ribbon form. The K133:K133 charge apposition is displayed in CPK space-filling form. Center to center distances in Å between the helix 5/5 and helix 4/6 pairs are indicated by double-headed arrows. Color code: proline, green; helix 5 (residues 121–142), pink; helix 4 (residues 99–120) and helix 6 (residues 143–164) are identified by red text. (D) Molecular dynamics (MD) simulation snapshot at 600 ps of apoA-I in the 129j double belt rotamer conformation on discoidal HDL. The molecular graphics models show the opening of a "mouth" between the helix 5–helix 5 antiparallel pair exposing the underlying fatty acyl chains.[40] The upper part of the Figure shows the 600 ps snapshot with the backbone apoA-I displayed in ribbon mode and the lipid in space-filling mode; the lower part of the Figure shows the 600 ps snapshot with both in space-filling mode. Upper: basic (blue) and acidic (red) residues in the more superficial positions, 9 and 5, respectively, are represented in stick mode. Basic (blue) and acidic (red) residues in the more deeply buried position 2 are represented in space-filling mode.[20] Proline residues in both models are colored yellow and displayed in space-filling mode. Color code for lipid: fatty acyl chains, black; phosphorus, gold; remainder of headgroups, red.

implies that both full-length and (Δ43)apoA-I share common structural elements in the domain of apoA-I that encircles the edges of both discs. Modeling shows that the R2-2 discs have a circumference equivalent to a (on average) continuous helical belt equal in length to residues 44–243 of apoA-I. It follows from this that the smaller R2-1 discs must contain a pairwise segment of this belt that is hinged away from the disc edge. The combination of molecular dynamics simulation,[40] determination of the lipid-affinity of synthetic peptide analogs of the 22mer tandem repeats,[35] and phylogenetic analysis by LOCATE support helix 5 as a likely candidate for the pairwise helical hinge on the edge of the R2-1 disc.

These results do not definitively support helix 5 as the location of the hinged domain. For one thing, the lipid surfaces used to measure the lipid-affinity of synthetic peptide analogs of helical repeats from apoA-I were largely flat and, further, the peptides were interacting with polar head group regions of bilayers rather than with the more open bilayer disc edge. Further, previous studies suggest locations other than helix 5 (although in its general vicinity) might be involved in hinge formation. Monoclonal antibody binding studies identified helix 4 and helix 5 as a mobile middle region,[31,45,46] a possibility supported by studies using limited proteolysis and NMR.[29,33] The results of a surface plasmon resonance study suggest that a region including helixes 5 and 6 forms the hinged domain.[47] Furthermore, recent studies of lipoprotein particles containing two or four apoA-I molecules associated with lipid vesicles labeled with photoactivable reagents suggest that a region containing helixes 3 and 4 swings away from the lipid surface.[34] Clearly, then, the definitive location of the hinged domain(s) of apoA-I has yet to be determined.

That the R2-1 particle undergoes little variation in diameter with changes in the DMPC:apoA-I molar ratio suggests a single hinged domain whose association/disassociation is essentially all-or-none, implying that a half-associated/half-disassociated hinged domain is energetically unfavorable. A more subtle "mouth"-shaped unfolding and refolding of helix 5 pairwise on the disc edge of the type observed during MD simulation of the 129j rotamer (Figure 9(D)) represents a dynamic structural change with but minimal effect on the diameter of the R2-1 disc.

The three larger discs, R2-3, R2-4 and R2-5, are not formed by (Δ43)apoA-I but can be reconstituted by addition of a peptide analog of the N-terminal 43 residue flexible domain, showing that the flexible domain is necessary and sufficient for formation of the three largest discs. The conformations of full-length apoA-I on these flexible domain-dependent discs model as the R2-2 conformation extended on the disc edge by one, two or three of the 11 residue tandem amphipathic helical repeats (termed G1, G2 and G3), respectively, contained within the flexible domain. Thus one, two and three of the 11mer G^* helixes of residues 1–43 must cover the 11, 22 and 33 residue gaps produced between the N-terminal and the C-terminal ends of the lipid-associating domain as the discs increase in size to form R2-3, R2-4 and R2-5, respectively.

Assuming a mean cross-sectional area for DMPC of 58–60 $Å^2$ in the disordered phase,[48,49] and a circumferential helical belt thickness of 10 Å, one can calculate the DMPC:apoA-I molar ratios for the R2-1, R2-2 and R2-3 discs at their maximal S_d of 98 Å, 105.5 Å and 110.5 Å to be 80–82 : 1, 96–99 : 1 and 107–111 : 1, respectively. At molar ratios of 100 : 1 or less, the R2-1, R2-2 and R2-3 particles are associated with the appearance of free apoA-I in an inverse DMPC concentration dependence. These results suggest a minimum lipid:protein stoichiometry requirement of approximately 110 for DMPC:AI complex formation (Figures 3(B) and 6). The similarity of this ratio to the calculated composition of the R2-3 discs suggests that DMPC addition beyond the saturation point would result in expansion of the R2-3 disc population and a corresponding decrease in the R2-1 disc population, an event confirmed in Figure 6.

To examine whether temperatures below and above the DMPC phase transition have significant effects on particle size, DMPC:apoA-I complexes were made and their size measured at two different temperatures (4 °C and 34 °C). Neither the temperature of particle formation nor the temperature of particle size measurement had any major effect on particle size and very little effect on particle distribution (data not shown). At first it might seem a bit surprising that temperature has such little effect on particle size. However, we have found that MD simulations provide an explanation for why particles with the same protein scaffolding (i.e. R2-2) but different lipid areas (condensed *versus* disordered DMPC) appear not to vary greatly in Stokes diameter on NDGGE (unpublished results). Further, the presence of the protein scaffolding may perturb the DMPC and prevent it from undergoing the ordered (condensed) phase transition.

The kinetics of R2 disc formation, in the absence of cholate, appears to be driven by the ability of nascent discs to take up bulk DMPC and transform themselves step-wise into larger discs (Figure 8). The ability of a free flexible domain in the form of the N43 peptide to interact with preformed R2-2 discs to create larger discs also suggests bulk lipid transfer as a mechanism for step-wise disc conversion (Figure 5). Interaction with preformed discs must initially be with the disc face and only later with the disc edge. The failure of discs preformed from full-length apoA-I to take up the N43 peptide supports this interpretation; i.e. the flexible domain of the full-length protein competitively inhibits the association of the peptide with the disc face. This process appears, however, to be limited by a kinetic barrier in the formation of R2-3 from R2-2 discs. In the absence of cholate, R2-2 remains a major particle even up to a molar ratio of 600 : 1 (Figure 3(A)), R2-4 and R2-5 never mature to their maximal S_d and R2-3 maintains a concentration less than that of R2-2.

However, in the presence of cholate, R2-2 becomes a minor particle at or above a molar ratio of 150 : 1. At the constant protein concentration used in the experiments of Figures 4 and 6, the R2-2 discs saturate at approximately 100 : 1 and, with additional DMPC, the mole fraction of apoA-I associated with the R2-2 disc decreases and that with the larger discs correspondingly increases. Presumably, the smaller discs take up excess DMPC to form the larger discs in a discontinuous transformation, a process driven by mass action. An understanding of the structural basis for the kinetic barrier between R2-2 and R2-3 will require an understanding of the structure and kinetics of the flexible domain.

Our working model for size heterogeneity is developed from studies of complexes of apoA-I with DMPC, a non-physiological lipid. Preliminary studies (data not shown) with the more physiological lipid 1-palmitoyl-2-oleoyl-phosphatidylcholine (POPC), show that five step-wise heterogeneous particles of similar mean size, R2-1 to R2-5, are produced by apoA-I complexes formed from POPC and DMPC. However, POPC:apoA-I bands seen on NDGGE are broader than DMPC:A-I bands produced under identical conditions. We postulate that the broadness of the POPC bands results from a slower rate of exchange between particles of the more hydrophobic POPC than that between particles of the more hydrophilic DMPC; a slower rate of lipid exchange would be expected to produce a broader distribution of kinetically trapped particles within each of the five step-wise heterogeneous particles, e.g. R2-2. Kinetic trapping has been suggested by Gursky and colleagues to be the basis for stability of native HDL particles.[50] A similar process of kinetic trapping appears to be the basis for stability of the larger step-wise heterogeneous DMPC:apoA-I particles (R2-3 to R2-5) produced by temperature cycling.

The flexible domain has an additional effect upon the R2 discs; in its presence R2-2 is significantly more prominent than R2-1, in its absence the reverse is true. Understanding the molecular mechanism for the flexible domain effect on the distribution of R2-2 *versus* R2-1, as well as the structural basis for the kinetic barrier between R2-2 and R2-3, will require an understanding of location and structure of the flexible domain in both discs. Possibilities for the organization of the flexible domain in these discoidal structures include: (i) unassociated with the disc as either random or helical coiled-coil; or (ii) associated with the phospholipid surface of the disc face as amphipathic α helixes or β strands. Our CD spectroscopic data show that complexes containing mostly R2-2 have less α helicity than complexes containing mostly R2-3 and R2-4 (Figure 7 and Table 1), indicating that lipid binding of the flexible domain leads to increased α helicity. Data from a recent lipid binding study of truncated apoA-I by Saito *et al.* suggest that residues 1–43 of apoA-I are in a predominantly non-helical conformation in the lipid-free state and form α helixes upon lipid binding.[51] We are hopeful that MD simulations currently underway will provide more information about the organization of the flexible domain in R2-1 and R2-2.

The current study provides no data from which to propose a working model for continuous size heterogeneity. This phenomenon requires a specific molecular mechanism for the apoA-I double belt structure to flexibly accommodate itself to continuous increases in discoidal phospholipid. MD simulations currently underway suggest several credible mechanisms for continuous size heterogeneity, one feature of which is the proline-induced kinking of the double belt observed in our previously published MD simulations.[40]

Double belt *versus* hairpin-belt models

We have assumed a double belt structure in our development of models for the R2 discoidal complexes of apoA-I with DMPC, but our conclusions are applicable just as well to one form of the hairpin-belt model. The hairpin-belt structure represents a variation on the basic topography of the double belt. The two models are so similar that the basic topographical signature, the helix–helix salt-bridges proposed to stabilize the helix–helix registry, is identical, except that the salt-bridges are intra-helical *versus* inter-helical for the hairpin-belt *versus* the double belt, respectively. Additionally, there are two possible conformations for a hairpin-belt model on the R2 discs: hairpin turn adjacent to hairpin turn (head to head) and hairpin turn adjacent to hairpin tail (head to tail).

Assuming identical salt-bridge patterns, a 129j double belt would be very difficult to distinguish topographically from a hairpin-belt with head to head orientation. The helical repeats in both the helical belts would be identical with one difference other than intramolecular *versus* intermolecular helix–helix contacts, the nature of the central helix 5–helix 5 contact (Figure 10, upper). Although both of these models juxtapose the G129 residues of the two apoA-I monomers, the juxtaposition in the R2-2 discs would be inter-helical for the 129j double belt and inter-turn for the corresponding hairpin-belt. For the R2-1 discs, assuming a hinged domain involving helix 5, the helix 5 pairwise hairpins would hinge away from the disc edge in directions parallel with *versus* perpendicular to the plane of the disc in the 129j double belt *versus* the head to head hairpin-belt models, respectively (Figure 10, lower). The hinge in the hairpin-belt model would create a short segment of intermolecular contact between the pairwise helix 5 hairpins.

The head to tail helical hairpin would have the same intra-apoA-I salt-bridge pattern as the head to head model. The major difference is that the order of helical repeats in the upper and lower belts would no longer be identical in the two models. Rather than the helical repeats from N terminus to C terminus proceeding as in the double belt, each belt

would be composed of two repeats of that portion of the apoA-I sequence N-terminal or C-terminal to helix 5. Further, the G129 residues of the two apoA-I monomers would be in contact with the helical-hairpin tails, not with themselves, thus making pairwise helix 5 hinging impossible in the head to tail model. For this reason, we consider the head to tail hairpin model unlikely for R2 discs.

Finally, since essentially all helix–helix interactions are intra-molecular, there is no easy way in the hairpin-belt model to generate the disulfide bonds known to link together the monomers of the natural cysteine mutations of apoA-I, apoA-I_{Milano} and apoA-I_{Paris};[52] disulfide bond formation is trivial in the double belt model. Both mutations occur in helical position 9 and thus, as we note elsewhere, are capable of approaching each other in the LL rotamer to within the minimal 6 Å required for disulfide bond formation.[20,52] Even if the disulfide bonds were to be formed in lipid-poor apoA-I dimers or following intrahelical hairpin "walking", the resultant dimer belt would be locked firmly in the double belt conformation.

While we consider the double belt model to be the more likely structure for the R2 discs, from our data we cannot rule out the hairpin turn, particularly the head to head version. A helical hairpin conformation is required for at least one of the apoA-I monomers on R3 discs and, further, this conformation requires less cooperativity for formation than the double belt, in that the folding of each monomeric hairpin is independent of the other monomer. However, since the *in vivo* structure of discoidal HDL depends uniquely upon a complex and not yet understood process of lipid accumulation that requires minimally the transmembrane protein, ABCA1,[4–8] the structure of *in vitro* discs may not precisely reflect circulating structures.

Biological implications

Our model may have interesting biological implications in apoA-I related processes such as activation of LCAT, ABCA1-induced discoidal HDL assembly, and interactions with SR-B1. In studies with apoA-I-mimic synthetic peptides[53] and site-directed mutations of apoA-I,[37] the LCAT-activating domain of apoA-I has been located to central helixes of apoA-I around helix 5. The opening and closing of the "mouth" between the helix 5–helix 5 pair from the disc surface may affect LCAT-activating ability of apoA-I and the access of lipid substrate by LCAT. Indeed, experimental evidence indicates that small HDL is more reactive with LCAT than large HDL.[47] It has been shown that a central apoA-I domain loosely bound to lipids in discoidal lipoproteins is capable of penetrating the bilayer of phospholipid vesicles,[34] suggesting the importance of the central domain in lipid exchange between HDLs and cell membranes. Recent *in vitro* and *in vivo* data all indicate that the N terminus and the central domain of apoA-I are important for LCAT activation and ABCA1-mediated lipid efflux and HDL biogenesis.[54,55]

A further point concerns the biological relevance of both the step-wise and continuous heterogeneity in apoA-I discoidal complexes. Since discoidal HDL is formed *in vivo* by interactions of lipid-poor apoA-I with ABCA1 on the cell membrane, an important question for the future is: do cholesterol-loaded cells, such as macrophages, induce differences in structure of ABCA1-assembled discoidal HDL compared with normal macrophages and, if so, what might be the biological implications?

Conclusion

These results provide a substantial starting point for studies underway that utilize site-directed mutagenesis and MD simulations to study the structure and function of discoidal (nascent) HDL particles and their mature product, circulating spheroidal HDL.

Materials and Methods

Identification and computational analysis within a given amino acid sequence

The program αLOCATE identifies potential amphipathic α helixes within an amino acid sequence using termination rules as described.[56] To be able to identify the presence of a class A amphipathic helix in a given amino acid sequence, a mathematically defined motif for the particular charge distribution associated with various classes of amphipathic helixes was derived,[57] and implemented in αLOCATE. The program creates either a linear or a two-dimensional plot. The two-dimensional plot displays the location of each sequence with the desired motif on the *y*-axis and a measure of Λα on the *x*-axis (see Figure 9(B)). Available options include minimum allowable cutoff values for amphipathic motif parameters, such as sequence length and Λα.

Rotamer nomenclature

For every unique rotamer registration, there are two, and only two, residues on opposite sides of apoA-I helical ring 1 that are juxtaposed with their complementary residues on helical ring 2. For example, for the two unique rotamers 129j and 133j, residue 129G or 133K on helix 1 is juxtaposed precisely normal to the plane of the ring pair with residue 129G or 133K on helix 2.

Expression and purification of recombinant apoA-I and (Δ43)apoA-I

Human full-length apoA-I or (Δ43)apoA-I cDNA in plasmid pGEMEX was expressed in *Escherichia coli* BL21/DE3 cells and purified as described.[16] Briefly, the expression of apoA-I was monitored by Western blotting analysis of the bacterial lysate with anti-human apoA-I antibody. The bacterial lysate containing mutant apoA-I was loaded onto a preparative reversed-phase HPLC (C_4) column, and proteins were eluted and separated by a gradient of acetonitrile with 0.1% (v/v) trifluoroacetic

acid. Preparative HPLC fractions containing apoA-I (identified by immuno-dot-blots) were then subjected to purity and identity analyses. The purity of expressed proteins was examined by analytical HPLC (C_{18}) and SDS-PAGE. The identity of the proteins was confirmed by mass spectrometry and N-terminal amino acid sequencing. Purified proteins were lyophilized and stored at −20 °C or −80 °C.

Preparation of wild-type and mutant apoA-I solutions

Lyophilized protein was solubilized in 6 M guanidine hydrochloride. The solubilized protein solution was loaded onto a desalting column (Econo-Pac 10DG Disposable Chromatography Columns, BioRad, Hercules, CA) and the protein was eluted by PBS (0.02 M sodium phosphate (pH 7.4), 0.15 M NaCl). An extinction coefficient of 1.13 ml/(mg cm) and 0.991 ml/(mg cm) at 280 nm was used for determining the concentration of full-length apoA-I and (Δ43)apoA-I, respectively, in 6 M guanidine hydrochloride.[16]

Preparation of phospholipids

Multilamellar vesicles (MLV) of DMPC were prepared as described.[58] Briefly, DMPC (Avanti Polar-Lipids, Alabaster, AL) was dissolved in chloroform and dried under a stream of N_2 in a pre-weighted glass tube with periodic mixing to form a lipid film on the wall of the tube. Upon complete removal of chloroform, PBS was added to give a final concentration of DMPC of 10 mg/ml. After hydration in the buffer for at least four hours, DMPC was dispersed by vortex mixing until a uniform, milky suspension was formed. This dispersion was used for preparation of discoidal apoA-I:DMPC complexes. For preparing DMPC:apoA-I or (Δ43)apoA-I complexes using the sodium cholate dialysis method,[58] sodium cholate in PBS was added into a tube containing dried DMPC to make a final concentration of DMPC of 10 mg/ml (the final sodium cholate to DMPC molar ratio was 2 : 1).

Preparation and analysis of discoidal DMPC:apoA-I complexes

MLV of DMPC were mixed with apoA-I or (Δ43) apoA-I in different molar ratios as needed. To equilibrate the protein–lipid interactions optimally, the lipid–protein mixture was subjected to four thermal cycles of 37 °C, 23 °C, and 20 °C with one hour at each temperature per cycle. After the thermal cycling, an aliquot of the complex was analyzed by NDGGE on a 4–20% gradient acrylamide gel in Tris-glycine (Invitrogen, Carlsbad, CA). The gels were stained with the colloidal blue staining kit (Invitrogen, Carlsbad, CA). With reference to protein molecular markers, the Stokes diameters (S_d) of different-sized particles in the complexes were calculated on the basis of density scans of the gels by LabWorks image acquisition and analysis software (UVP Inc., Upland, CA). In addition, DMPC:apoA-I or (Δ43)apoA-I complexes were prepared by the sodium cholate dialysis procedure.[58] Briefly, DMPC in sodium cholate solution was mixed with apoA-I or (Δ43) apoA-I in different molar ratios as needed. After four thermal cycles as described above, the mixture was dialyzed against PBS overnight at 4 °C with at least six changes of 1 l each and then subjected to NDGGE analysis. The protein and lipid contents of the complexes were determined after dialysis by a modified version of the Lowry protein assay,[59] and a phospholipid enzymatic assay (Wako Chemicals USA Inc., Richmond, VA), respectively.

Circular dichroism spectroscopy

The CD spectroscopy was conducted as described.[16,36] Briefly, the CD spectra were recorded using an AVIV 62DS spectropolarimeter (Lakewood, NJ) equipped with a thermoelectric temperature-controller and interfaced to a personal computer. The instrument was calibrated with (1S)-(+)-10-camphorsulfonic acid. The CD spectra were measured with apoA-I or (Δ43)apoA-I in solution (PBS) or in DMPC complexes from 260 nm to 190 nm every 0.5 nm with 4 seconds averaging per point and a 2 nm bandwidth. A 0.01 cm path-length cell was used for obtaining the spectra. The CD spectra were signal-averaged by adding four baseline-corrected scans. All the CD spectra were recorded at 25 °C with protein concentration of 7.7 μM. We have confirmed that the spectra were concentration-independent in the concentration range of 2.5–25 μM for both apoA-I and (Δ43)apoA-I.[16]

The mean residue ellipticity, $[\theta]_{MRE}$ (deg cm^2 dmol^{-1}), was calculated using the following equation:

$$[\theta]_{MRE} = (MR \times \theta)/(10cl)$$

where, MR is the mean residue mass (calculated as the molecular mass of the protein divided by the number of amino acid residues in the protein), θ is the observed ellipticity (in degrees), c is the concentration of the protein (in g ml^{-1}), and l is the pathlength of the cell (in cm). The percentage helicity (% α-helix) of the protein was estimated from the following equation:

$$\%\alpha - \text{helix} = ([\theta]_{222} + 3000)/(36000 + 3000) \times 100$$

where $[\theta]_{222}$ is the mean residue ellipticity at 222 nm.[60]

Acknowledgements

We thank Dr David W. Garber for technical assistance in iodination of peptides. We thank Drs Michael J. Jablonsky, Donald D. Muccio, and Manjula Chaddha for their assistance in CD spectroscopy. This work was supported, in part, by the National Institutes of Health grant P01 HL-34343 (to J.P.S.).

References

1. Wilson, P. W., Abbott, R. D. & Castelli, W. P. (1988). High density lipoprotein cholesterol and mortality. The Framingham heart study. *Arteriosclerosis*, **8**, 737–741.
2. Segrest, J. P. & Anantharamaiah, G. M. (1994). Pathogenesis of atherosclerosis. *Curr. Opin. Cardiol.* **9**, 404–410.
3. Sloop, C. H., Dory, L., Krause, B. R., Castle, C. & Roheim, P. S. (1983). Lipoproteins and apolipoproteins in peripheral lymph of normal and cholesterol-fed dogs. *Atherosclerosis*, **49**, 9–21.
4. Brooks-Wilson, A., Marcil, M., Clee, S. M., Zhang, L. H., Roomp, K., van Dam, M. *et al*. (1999). Mutations in ABC1 in Tangier disease and familial high-density lipoprotein deficiency. *Nature Genet.* **22**, 336–345.

5. Bodzioch, M., Orso, E., Klucken, J., Langmann, T., Bottcher, A., Diederich, W. *et al*. (1999). The gene encoding ATP-binding cassette transporter 1 is mutated in Tangier disease. *Nature Genet.* **22**, 347–351.
6. Rust, S., Rosier, M., Funke, H., Real, J., Amoura, Z., Piette, J. C. *et al*. (1999). Tangier disease is caused by mutations in the gene encoding ATP-binding cassette transporter 1. *Nature Genet.* **22**, 352–355.
7. Remaley, A. T., Rust, S., Rosier, M., Knapper, C., Naudin, L., Broccardo, C. *et al*. (1999). Human ATP-binding cassette transporter 1 (ABC1): genomic organization and identification of the genetic defect in the original Tangier disease kindred. *Proc. Natl Acad. Sci. USA*, **96**, 12685–12690.
8. Lawn, R. M., Wade, D. P., Garvin, M. R., Wang, X., Schwartz, K., Porter, J. G. *et al*. (1999). The Tangier disease gene product ABC1 controls the cellular apolipoprotein-mediated lipid removal pathway [see comments]. *J. Clin. Invest.* **104**, R25–R31.
9. Francis, G. A., Knopp, R. H. & Oram, J. F. (1995). Defective removal of cellular cholesterol and phospholipids by apolipoprotein A-I in Tangier disease. *J. Clin. Invest.* **96**, 78–87.
10. Segrest, J. P., Garber, D. W., Brouillette, C. G., Harvey, S. C. & Anantharamaiah, G. M. (1994). The amphipathic alpha helix: a multifunctional structural motif in plasma apolipoproteins. *Adv. Protein Chem.* **45**, 303–369.
11. Segrest, J. P., Jackson, R. L., Morrisett, J. D. & Gotto, A. M. (1974). A molecular theory of lipid–protein interactions in the plasma lipoproteins. *FEBS Letters*, **38**, 247–258.
12. Segrest, J. P., Jones, M. K., De Loof, H., Brouillette, C. G., Venkatachalapathi, Y. V. & Anantharamaiah, G. M. (1992). The amphipathic helix in the exchangeable apolipoproteins: a review of secondary structure and function. *J. Lipid Res.* **33**, 141–166.
13. Wlodawer, A., Segrest, J. P., Chung, B. H., Chiovetti, R. & Weinstein, J. N. (1979). High-density lipoprotein recombinants: evidence for a bicycle tire micelle structure obtained by neutron scattering and electron microscopy. *FEBS Letters*, **104**, 231–235.
14. Atkinson, D., Small, D. M. & Shipley, G. G. (1980). X-ray and neutron scattering studies of plasma lipoproteins. *Ann. N Y Acad. Sci.* **348**, 284–298.
15. Segrest, J. P. (1977). Amphipathic helixes and plasma lipoproteins: thermodynamic and geometric considerations. *Chem. Phys. Lipids*, **18**, 7–22.
16. Rogers, D. P., Brouillette, C. G., Engler, J. A., Tendian, S. W., Roberts, L., Mishra, V. K. *et al*. (1997). Truncation of the amino terminus of human apolipoprotein A-I substantially alters only the lipid-free conformation. *Biochemistry*, **36**, 288–300.
17. Tricerri, M. A., Behling Agree, A. K., Sanchez, S. A., Bronski, J. & Jonas, A. (2001). Arrangement of apolipoprotein A-I in reconstituted high-density lipoprotein disks: an alternative model based on fluorescence resonance energy transfer experiments. *Biochemistry*, **40**, 5065–5074.
18. Tall, A. R., Small, D. M., Deckelbaum, R. J. & Shipley, G. G. (1977). Structure and thermodynamic properties of high density lipoprotein recombinants. *J. Biol. Chem.* **252**, 4701–4711.
19. Borhani, D. W., Rogers, D. P., Engler, J. A. & Brouillette, C. G. (1997). Crystal structure of truncated human apolipoprotein A-I suggests a lipid-bound conformation. *Proc. Natl Acad. Sci. USA*, **94**, 12291–12296.
20. Segrest, J. P., Jones, M. K., Klon, A. E., Sheldahl, C. J., Hellinger, M., De Loof, H. & Harvey, S. C. (1999). A detailed molecular belt model for apolipoprotein A-I in discoidal high density lipoprotein. *J. Biol. Chem.* **274**, 31755–31758.
21. Koppaka, V., Silvestro, L., Engler, J. A., Brouillette, C. G. & Axelsen, P. H. (1999). The structure of human lipoprotein A-I. Evidence for the "belt" model. *J. Biol. Chem.* **274**, 14541–14544.
22. Maiorano, J. N. & Davidson, W. S. (2000). The orientation of helix 4 in apolipoprotein A-I-containing reconstituted high density lipoproteins. *J. Biol. Chem.* **275**, 17374–17380.
23. Panagotopulos, S. E., Horace, E. M., Maiorano, J. N. & Davidson, W. S. (2001). Apolipoprotein A-I adopts a belt-like orientation in reconstituted high density lipoproteins. *J. Biol. Chem.* **276**, 42965–42970.
24. Li, H., Lyles, D. S., Thomas, M. J., Pan, W. & Sorci-Thomas, M. G. (2000). Structural determination of lipid-bound ApoA-I using fluorescence resonance energy transfer. *J. Biol. Chem.* **275**, 37048–37054.
25. Li, H. H., Lyles, D. S., Pan, W., Alexander, E., Thomas, M. J. & Sorci-Thomas, M. G. (2002). ApoA-I structure on discs and spheres. Variable helix registry and conformational states. *J. Biol. Chem.* **277**, 39093–39101.
26. Davidson, W. S. & Hilliard, G. M. (2003). The spatial organization of apolipoprotein A-I on the edge of discoidal high density lipoprotein particles: a mass specrometry study. *J. Biol. Chem.* **278**, 27199–27207.
27. Oda, M. N., Forte, T. M., Ryan, R. O. & Voss, J. C. (2003). The C-terminal domain of apolipoprotein A-I contains a lipid-sensitive conformational trigger. *Nature Struct. Biol.* **10**, 455–460.
28. Brouillette, C. G., Jones, J. L., Ng, T. C., Kercret, H., Chung, B. H. & Segrest, J. P. (1984). Structural studies of apolipoprotein A-I/phosphatidylcholine recombinants by high-field proton NMR, nondenaturing gradient gel electrophoresis, and electron microscopy. *Biochemistry*, **23**, 359–367.
29. Calabresi, L., Tedeschi, G., Treu, C., Ronchi, S., Galbiati, D., Airoldi, S. *et al*. (2001). Limited proteolysis of a disulfide-linked apoA-I dimer in reconstituted HDL. *J. Lipid Res.* **42**, 935–942.
30. Roberts, L. M., Ray, M. J., Shih, T. W., Hayden, E., Reader, M. M. & Brouillette, C. G. (1997). Structural analysis of apolipoprotein A-I: limited proteolysis of methionine-reduced and -oxidized lipid-free and lipid-bound human apo A-I. *Biochemistry*, **36**, 7615–7624.
31. Bergeron, J., Frank, P. G., Scales, D., Meng, Q. H., Castro, G. & Marcel, Y. L. (1995). Apolipoprotein A-I conformation in reconstituted discoidal lipoproteins varying in phospholipid and cholesterol content. *J. Biol. Chem.* **270**, 27429–27438.
32. Calabresi, L., Vecchio, G., Frigerio, F., Vavassori, L., Sirtori, C. R. & Franceschini, G. (1997). Reconstituted high-density lipoproteins with a disulfide-linked apolipoprotein A-I dimer: evidence for restricted particle size heterogeneity. *Biochemistry*, **36**, 12428–12433.
33. Okon, M., Frank, P. G., Marcel, Y. L. & Cushley, R. J. (2002). Heteronuclear NMR studies of human serum apolipoprotein A-I. Part I. Secondary structure in lipid-mimetic solution. *FEBS Letters*, **517**, 139–143.
34. Corsico, B., Toledo, J. D. & Garda, H. A. (2001). Evidence for a central apolipoprotein A-I domain loosely bound to lipids in discoidal lipoproteins that is capable of penetrating the bilayer of phospholipid vesicles. *J. Biol. Chem.* **276**, 16978–16985.
35. Palgunachari, M. N., Mishra, V. K., Lund-Katz, S., Phillips, M. C., Adeyeye, S. O., Alluri, S. *et al*. (1996). Only the two end helixes of eight tandem

amphipathic helical domains of human apo A-I have significant lipid affinity. Implications for HDL assembly. *Arterioscler. Thromb. Vasc. Biol.* **16**, 328–338.
36. Mishra, V. K., Palgunachari, M. N., Datta, G., Phillips, M. C., Lund-Katz, S., Adeyeye, S. O. *et al*. (1998). Studies of synthetic peptides of human apolipoprotein A-I containing tandem amphipathic alpha-helixes. *Biochemistry*, **37**, 10313–10324.
37. Sorci-Thomas, M., Kearns, M. W. & Lee, J. P. (1993). Apolipoprotein A-I domains involved in lecithin-cholesterol acyltransferase activation. Structure:function relationships. *J. Biol. Chem.* **268**, 21403–21409.
38. Laccotripe, M., Makrides, S. C., Jonas, A. & Zannis, V. I. (1997). The carboxyl-terminal hydrophobic residues of apolipoprotein A-I affect its rate of phospholipid binding and its association with high density lipoprotein [published erratum appears in J. Biol. Chem. 1998 Jun 19;273(25):15878]. *J. Biol. Chem.* **272**, 17511–17522.
39. Burgess, J. W., Frank, P. G., Franklin, V., Liang, P., McManus, D. C., Desforges, M. *et al*. (1999). Deletion of the C-terminal domain of apolipoprotein A-I impairs cell surface binding and lipid efflux in macrophage. *Biochemistry*, **38**, 14524–14533.
40. Klon, A. E., Segrest, J. P. & Harvey, S. C. (2002). Molecular dynamics simulations on discoidal HDL particles suggest a mechanism for rotation in the apo A-I belt model. *J. Mol. Biol.* **324**, 703–721.
41. Blundell, T., Barlow, D., Borkakoti, N. & Thornton, J. (1983). Solvent-induced distortions and the curvature of alpha-helices. *Nature*, **306**, 281–283.
42. Pauling, L. & Corey, R. B. (1951). Atomic coordinates and structure factors for two helical configurations of polypeptide chains. *Proc. Natl Acad. Sci. USA*, **37**, 235–240.
43. Bussell, R. & Eliezer, D. (2003). A structural and functional role for 11-mer repeats in alpha-synuclein and other exchangeable lipid binding proteins. *J. Mol. Biol.* **329**, 763–778.
44. Jao, C. C., Der-Sarkissian, A., Chen, J. & Langen, R. (2004). From the cover: Structure of membrane-bound {alpha}-synuclein studied by site-directed spin labeling. *Proc. Natl Acad. Sci. USA*, **101**, 8331–8336.
45. Marcel, Y. L., Provost, P. R., Koa, H., Raffai, E., Dac, N. V., Fruchart, J. C. & Rassart, E. (1991). The epitopes of apolipoprotein A-I define distinct structural domains including a mobile middle region. *J. Biol. Chem.* **266**, 3644–3653.
46. Calabresi, L., Meng, Q. H., Castro, G. R. & Marcel, Y. L. (1993). Apolipoprotein A-I conformation in discoidal particles: evidence for alternate structures. *Biochemistry*, **32**, 6477–6484.
47. Curtiss, L. K., Bonnet, D. J. & Rye, K. A. (2000). The conformation of apolipoprotein A-I in high-density lipoproteins is influenced by core lipid composition and particle size: a surface plasmon resonance study. *Biochemistry*, **39**, 5712–5721.
48. Moore, P. B., Lopez, C. F. & Klein, M. L. (2001). Dynamical properties of a hydrated lipid bilayer from a multinanosecond molecular dynamics simulation. *Biophys. J.* **81**, 2484–2494.
49. Petrache, H. I., Tristram-Nagle, S. & Nagle, J. F. (1998). Fluid phase structure of EPC and DMPC bilayers. *Chem. Phys. Lipids*, **95**, 83–94.
50. Mehta, R., Gantz, D. L. & Gursky, O. (2003). Human plasma high-density lipoproteins are stabilized by kinetic factors. *J. Mol. Biol.* **328**, 183–192.
51. Saito, H., Dhanasekaran, P., Nguyen, D., Deridder, E., Holvoet, P., Lund-Katz, S. & Phillips, M. C. (2004). {alpha}-Helix formation is required for high affinity binding of human apolipoprotein A-I to lipids. *J. Biol. Chem.* **279**, 20974–20981.
52. Klon, A. E., Jones, M. K., Segrest, J. P. & Harvey, S. C. (2000). Molecular belt models for the apolipoprotein A-I Paris and Milano mutations. *Biophys. J.* **79**, 1679–1685.
53. Anantharamaiah, G. M., Venkatachalapathi, Y. V., Brouillette, C. G. & Segrest, J. P. (1990). Use of synthetic peptide analogues to localize lecithin: cholesterol acyltransferase activating domain in apolipoprotein A-I. *Arteriosclerosis*, **10**, 95–105.
54. Scott, B. R., McManus, D. C., Franklin, V., McKenzie, A. G., Neville, T., Sparks, D. L. & Marcel, Y. L. (2001). The N-terminal globular domain and the first class A amphipathic helix of apolipoprotein A-I are important for lecithin:cholesterol acyltransferase activation and the maturation of high density lipoprotein *in vivo*. *J. Biol. Chem.* **276**, 48716–48724.
55. Chroni, A., Liu, T., Gorshkova, I., Kan, H. Y., Uehara, Y., Von Eckardstein, A. & Zannis, V. I. (2003). The central helices of ApoA-I can promote ATP-binding cassette transporter A1 (ABCA1)-mediated lipid efflux. Amino acid residues 220–231 of the wild-type ApoA-I are required for lipid efflux *in vitro* and high density lipoprotein formation *in vivo*. *J. Biol. Chem.* **278**, 6719–6730.
56. Segrest, J. P., Jones, M. K., Mishra, V. K., Anantharamaiah, G. M. & Garber, D. W. (1994). apoB-100 has a pentapartite structure composed of three amphipathic alpha-helical domains alternating with two amphipathic beta-strand domains. Detection by the computer program LOCATE. *Arterioscler. Thromb.* **14**, 1674–1685.
57. Hazelrig, J. B., Jones, M. K. & Segrest, J. P. (1993). A mathematically defined motif for the radial distribution of charged residues on apolipoprotein amphipathic alpha helixes. *Biophys. J.* **64**, 1827–1832.
58. Jonas, A. (1986). Reconstitution of high-density lipoproteins. *Methods Enzymol.* **128**, 553–582.
59. Markwell, M. A., Haas, S. M., Bieber, L. L. & Tolbert, N. E. (1978). A modification of the Lowry procedure to simplify protein determination in membrane and lipoprotein samples. *Anal. Biochem.* **87**, 206–210.
60. Morrisett, J. D., Sparrow, J. T., Hoff, H. F. & Gotto, A. M. (1973). Methods for studying lipid-protein interactions. *Cardiovasc. Res. Cent. Bull.* **12**, 39–51.
61. Mishra, V. K. & Palgunachari, M. N. (1996). Interaction of model class A1, class A2, and class Y amphipathic helical peptides with membranes. *Biochemistry*, **35**, 11210–11220.
62. Sayle, R. A. & Milner-White, E. J. (1995). RASMOL: biomolecular graphics for all. *Trends Biochem. Sci.* **20**, 374.

Edited by G. von Heijne

(Received 10 June 2004; received in revised form 24 August 2004; accepted 10 September 2004)